Ph.D. Dissertation

A Novel Antibody Screening Method for Detection of Rare Antibodies

희귀 항체 발굴을 위한

새로운 항체 스크리닝 방법

2020 년 2 월

DEPARTMENT OF ELECTRICAL AND

COMPUTER ENGINEERING

SEOUL NATIONAL UNIVERSITY

SEOHEE CHANG

A Novel Antibody Screening Method for Detection of Rare Antibodies

지도 교수 권 성 훈

이 논문을 공학박사 학위논문으로 제출함

2020 년 2 월

서울대학교 대학원

전기 · 컴퓨터공학부

장 서 희

장서희의 공학박사 학위논문을 인준함

2020 년 2 월

위 원 장 정 준 호 (인)

부위원장 권 성 훈 (인)

위 원 심 현 보 (인)

위 원 김 지 윤 (인)

위 원 최 정 일 (인)

Abstract

A Novel Antibody Screening Method for Detection of Rare Antibodies

The success rate of biologics, especially antibody drugs, is increasing due to the development of biotechnology, which is augmenting the interest of pharmaceutical companies. Antibody drugs are leading the pharmaceutical market, and are predicted to grow with a CAGR 12.8% over the next 5~6 years. One of the obstacles in the early stage of antibody-drug discovery is the selection of a few potential antibodies among the billions of candidates.

Phage display is the most widely used technology for screening antibody libraries in therapeutic drug discovery. A variety of antibodies encoded in the form of phagemid library can be displayed on the surface of phage, providing genotype-

to-phenotype linkage, making them a useful tool for antibody selection and identification. The biopanning process selectively enriches a set of antibodies having high affinity to a given antigen, so that the best binders can be taken amongst a number of potential candidates after experiencing multiple rounds of biopanning. The tremendous screening capability, along with several advantages such as the capacity to screen large libraries, easy manipulation, and low cost of propagation, has made phage display the most powerful tool for antibody drug discovery.

Despite such advantages, phage display technology has technical limits, such as time-consuming, laborious work, the limited screen size, and loss of binders. First, the laborious colony picking and functional testing of individual phages clones limit the screen size to hundreds compared to the size of the whole library(>10^9). Due to this limited screen size, multiple rounds of biopanning are required for sufficient enrichment of positive clones, which take from two weeks to a month. Automated procedures were developed for reducing laborious work with a multichannel pipetting device and 96well plate, but these methods do not extend the screen size

enough to eliminate multiple rounds of biopanning. There is also a loss of binders in each panning step. Insufficient elution causes the loss of high-affinity binders, and the amplification bias leads to the loss of rare binders. The use of magnetic beads that offers an increased surface area minimizes the loss in the binding step but does not have an impact on the other steps. The high-throughput method in the whole panning step is needed to reduce multiple rounds of biopanning for minimization of time-consuming, laborious work, and the loss of binders.

There have been many efforts to adopt microtechnologies to make advances in the field of bioscience. For phage display applications, especially, various single-cell level analyses were developed to both minimize amplification bias and maximize the throughput of analysis, thereby reducing the number of panning rounds. By employing a microcapillary device having densely-packed microreaction chambers, more than one million antibody clones were successfully screened at once. A microfluidic device was also utilized to generate water-in-oil microemulsion reaction chambers, increasing the analysis throughput to infinite in theory. Although both

methods could reduce the number of required panning rounds with extremely high throughput, complicated sample isolation approaches are needed to be accompanied. In addition, both methods are prone to possible sample cross-contamination at sample retrieval.

In this dissertation, a high-throughput phage display technology using a microwell array chip and an automated laser-driven sample retrieval system has been developed. The use of the single-cell level approach in combination with an elaborate sample retrieval method enables high-throughput sample retrieval at minimal amplification bias as well as sample cross-contamination. Using the developed phage display platform, screening of synthetic deimmunization library is demonstrated, obtaining novel antibody clones that were not detectable in the conventional biopanning method.

Keywords: High-throughput phage display, microwell array, automated system, antibody screening

Student Number: 2013-23138

Table of Contents

ABSTRACT III

TABLE OF CONTENTS VII

LIST OF TABLES X

LIST OF FIGURES XI

CHAPTER 1. INTRODUCTION 1

1.1. The Therapeutic Antibody Market 2

1.1.1. Market Trends for therapeutic antibody 2

1.1.2. The Development Process of Therapeutic Antibody 4

1.2. Conventional Antibody Library Screening Method 6

1.2.1. Phage display 6

1.2.2. Difficulties in conventional phage display 10

1.2.3. Previous researches on phage display technology applied the high-throughput methods from other 14

1.3. Main Concept: a technology for high-throughput phage display using a microwell array chip and automated retrieval system 16

1.3.1. My Works in This Dissertation 18

CHAPTER 2. SYSTEM DEVELOPMENT 20

2.1. Preparation of phage display and microwell array chip 22

2.1.1. PDMS microwell array for long-time cell culturing 22

2.1.2. The single-cell loading condition in the microwell 25

2.1.3. Design of holder by a hybrid structure 28

2.2. Detection of target samples 31

2.2.1. Independent substrates for detection and retrieval 31

2.2.2. Automated imaging process 33

2.3. Retrieval of target samples 35

2.3.1. The phage capturing layer for retrieval using laser 35

2.3.2. The automated laser-driven sample retrieval system 41

2.4. Analysis of genotype and phenotype of retrieved samples 44

2.4.1. The high-throughput analysis of retrieved clones 44

2.5. Validation of the whole process 46

2.5.1. Validation test in various positive rate libraries 46

2.5.2. Validation test in each panning round library - from 1st to 4th 49

CHAPTER 3. APPLICATION: SCREENING OF DEIMMUNIZATION LIBRARY 51

3.1. Therapeutic Benefit of the deimmunization 52

3.2. Screening of Deimmunization library against CD28 antigen using the proposed high-throughput phage display method 53

3.2.1. Experimental procedure 53

3.2.2. The results of Screening of Deimmunization library using the proposed high-

throughput phage display 59

CHAPTER 4. CONCLUSION AND DISCUSSION 68

BIBLIOGRAPHY 71

국문 초록 75

List of Tables

Table 2.1 The results of analyzed the fourth round panning library by proposed platform. 123 clones out of isolated 137 clones were five unique sequences and identified as positive clones in the conventional phage display method. 50

Table 3.1 Amino acids available at each mutation site. A pre-discovered anti-CD28 scFv clone was selected as a randomization template in which five amino acid sites were mutated (RMN/YMY/NNK/MTN/RYN)..... 58

Table 3.2 The results of NGS in TR™ analysis. As a result of sequencing, 203 out of retrieved 318 clones were analyzed, and among 112 clones were positive clones.. 62

Table 3.3 The results of NGS in TR™ analysis based on counts. When the counts were more than 3, the positive rate was 80%, and when the counts were lower than 2, only half of the clones were positive. 63

Table 3.4 The possible amino acids in five mutation sites. Red letters were the most frequenct amino acids in the result of screening by the proposed platform…. 64

List of Figures

Figure 1.1 Market trends for therapeutic antibody. (a) Salse of biologics by product type. Note that recombinant proteins were increased ~26% between 2008 and 2013, but monoclonal antibodies were increased ~90% (Reprinted from [2]). (b) Highest-selling drugs in 2018. Five out of the top 10 drugs were antibody drugs (Reprinted from [3]). 3

Figure 1.2 Drug-development cycle and the 'valley of death'. Capitalized cost over 13.5 years is $1.8 billion per launch. The cost and time are most consumed in the target validation and lead selection process[6]. 5

Figure 1.3 Structure of antibody. (a) Composition of antibody[9]. Antibody couples light chains and heavy chains. The variable regions, antigen-binding site, includes the ends of the light and heavy chains. (b) Variability of residues in variable regions. Within light and heavy chains, three CDRs and four FRs exist [10]. 6

Figure 1.4 scFv structure and DNA recombination in phage display technology. The VH and VL domain are linked to form scFv. scFv is expressed on the surface of phage along with geneIII protein(reprinted from [12]). 8

Figure 1.5 The phage display cycle. Specific clones are captured by binding to antigen, and non-specific clones are removed by washing, followed by elution. Phages are amplified by infection and regrowth of phage-producing cells between panning rounds. 9

Figure 1.6 Selection of antibody and timeline of phage display. Almost two weeks are consumed for three rounds of panning(Reprinted from [16]). 10

Figure 1.7 Elution methods in panning round. Specific binders to the antigen are released by elution methods. Acid or basic elution is usually used.

Competitive elution and directly infecting E. coli method are also used[18]. 11

Figure 1.8 The bias in the amplification step. (a) Affinity and growth rate are independent. (b) Phages that bind to the specific antigen are selected, and non-specific binders are also selected. (c) The amplification step further enriches clones that have a growth advantage. 12

Figure 1.9 Diagram of changes in the size of library during three rounds of panning. After three rounds of panning, the screen identifies binders. The number of identified binders, however, is much smaller than the number of binders that were originally present in the library.. 13

Figure 1.10 Schematic of the microcapillary method. Single cells are captured in densely packed microcapillary arrays and sealed. Target capillaries are automatically identified, and cells are recovered by the pneumatic pressure(reprinted from [28]). 15

Figure 1.11 Diagram of the micro-emulsion method. Cells are compartmentalized with antigen-coated beads in a water-in-oil emulsion. The emulsion is broken, and the beads are collected. The labeled beads can be sorted by flow cytometry(reprinted from [27]). 16

Figure 1.12 Main concept of proposed technology: A high-throughput phage display using a microwell array chip and automated laser retrieval system. (a) Phage-infected cells added to the microwell array. (b) The microwell array was mounted on the chip holders with the target-capturing substrate in order to isolate individual microwells. Phages were secreted from cells and captured. (c) After overnight incubation, the microwell array chip was disassembled. Cells and non-specific binders were removed, and captured phages on the microwell array were labeled. The position information of captured phage on the microwell array was transferred to the target-capturing substrate. (d) The obtained positions of the target samples were retrieved by using the automated laser retrieval system. Retrieved phages were lysed, and encoded antibody sequences were amplified by PCR. (e) High-throughput sequencing was

performed by using TrueRepertoire™(Celemics)[33]. (d) For validation of retrieved phages, phage-ELISA was performed. 17

Figure 2.1 System Overview. In chapter 2, the entire development process of the proposed technology will be described by dividing it into five parts. (1) How to prepare phage display and microwell array chip? (2) How to detect target samples? (3) How to retrieve target samples? (4) How to analyze retrieved clones? (5) How to validate the proposed technology? will be described…. 21

Figure 2.2 The fabrication of micropatterend slabs of PDMS. (a, b) The photoresist is spin-coated on a silicon wafer. (c) A mask is placed in contact with the layer of photoresist. (d) The photoresist is illuminated with ultraviolet (UV) light through the mask. An organic solvent dissolves and removes photoresist that is not crosslinked. (e) PDMS is poured on the master, cured thermally, and peeled away. (f) The resulting layer of PDMS has microstructures embossed in its surface (reprinted from [35]). 22

Figure 2.3 The bright field images show PDMS microwell array. The microwell array was consists of 113,000 wells and largely divided into 200 blocks of 20 x 10, with one block of 27 x 21 microwells(d 60μm, h 40μm). Each block had position markers (x, y). 24

Figure 2.4 The fluorescence images show that occupied cells were grown sufficiently during 19 hours of incubation. Bacteria expressing GFP and RFP, respectively, were loaded and incubated..... 24

Figure 2.5 The average number of cells in one well and the ratio of wells occupied by single-cell based on Poisson distribution. When the average of 0.1 cells was entered in one well, 95% of occupied wells are under the single-cell.. 26

Figure 2.6 The input concentration of cells and the average number of trapped cells/well based on Poisson distribution. The average number of trapped cells/well was calculated according to the Poisson distibution based on the ratio of wells occupied by the cells in the total chips. Input concentration of

cells and the output concentration of cells had a linear proportional relation. If the input concentration of cells was 0.02, the average of 0.1cells could be entered in one well(10% of the wells occupied) that fulfill a single-cell condition. 27

Figure 2.7 The deformation of the microwell array chip in the window-type aluminum plate holder. (a) Perfectly sealed microwells. (b) Deformation of microwell array and the cells out of well. 29

Figure 2.8 The structure of the hybrid holder. (a) Schematic representation of the holder. (b) Image of the holder. The holder consisted of an aluminum plate and an acryl sheet and was designed to a size of 96well plate. 30

Figure 2.9 The independent process of microwell array and sample-capturing substrate. The microwell array was used for target imagning and the sample-capturing substrate was used to isolate target samples. The target positions analyzed from microwell array images were applied to sample-capturing.. 31

Figure 2.10 The bright-field image of the assembled microwell array chip. After labeling, the fluorescence images of the microwell array and sample-capturing substrate, and isolated surface of sample-capturing substarte.(Black arrow: well occupied by cells with no fluorescence signal, red arrow: well occupied by cells with fluorescence signal) 32

Figure 2.11 Schematic of deriving target position. The image acquisition process was performed before and after the disassembly of the microwell array chip, respectively. The target well position (x, y) was obtained from labeled microwell array. Relative position was derived from image of assembled chip. 34

Figure 2.12 GUI program for obtaining target position on labeled microwell array and relative position from assembled microwell array chip. 35

Figure 2.13 (a) Fluorescence image of PS substrate. (b) PS fragment for phage retrieval, about 600 spots in the 2.4mm x 2.6mm area. Among them, 200 spots were positive clones. 36

Figure 2.14 Schematic of the PS pallet in microwell model. (a) The microwell array containing PS pallets performs target imaging and recovery from the microwells. (b) Scheamtic of the fabrication process. (i) A PDMS microwell array (shown in gray) is fabricated by a standard molding process. (ii) A polymer solution (shown in purple) is added to the PDMS microwell array. (iii) The wetted PDMS mold is immersed in the polymer solution and then slowly withdrawn. (iv) The dewetting of polymer solution from PDMS results in isolated convex polymer solution in each well. (v) Evaporation of solvent results in concave polymer microrafts inside each well(reprinted from [37]) 37

Figure 2.15 The results of the PS pallet model. (a) Confocal imaged of the PS pallet. The deformation of micowell was caused by PS pallet. (b) Fluorescence image of labeled microwell array containing the PS pallet. The quality of image was low because of the gap between microwell and PS pallet. (c) The results of pallet retreival method using gel electrophoresis. There were contaminzation during the sample retrieval. 38

Figure 2.16 The before and after images of disassembled microwell array in agarose pillar model. After overnight drying, agarose pallets were transferred to sample-capturing substrate. Because of residual agarose in microwell array, false positive was detected..... 39

Figure 2.17 Schematic of isolation process. The sacrificial layer absorbed the layer energy and vaporated to punch the sample-capturing substrate..... 40

Figure 2.18 Schematic of automated laser-driven sample retrieval system. Targeted samples were isolated by infrared laser system to 8-strip PCR tube conining lysis buffer, and then isolated phages were lysed and amplified by PCR. To confirm sequences of retreieved phages, obataind clones were sequenced by the Sanger method. 42

Figure 2.19 (a) The results of gel electrophoresis. Every selected clones were successfully isolated and amplified. (b) The results of the Sanger sequencing. Only CDRs had variability that suggsted there was no damage in the antibody

sequence during laser isolation. 43
Figure 2.20 Schametic of high-throughput analysis of collected phages. The isolated phages collected into one tube for one-step vector transformation. After the transfection of prepared phagemid, cells were individualized by TR™. Individulized colonies were sequences by barcoded PCR and NGS and measured the affinity agatinst target antigen using phage-ELISA. 45
Figure 2.21 The positive clones was mixed at a 1:0, 1:10, 1:100 ratio with the negative clone. (a) As the positive rate decrease, the number of wells with fluorescence signal was also decreased. (black arrow: wells occupied by cells, red arrow: fluorescence signal of wells) (b) The number of high-intensity clones were shifted to low-intensity. 47
Figure 2.22 The alignment of sequences analyzed by the Sanger sequencing. The selected clones were three positive clones with approximately 3:1:2 ratio (1:1:1 ratio in the input mix), no negative clone. Since the output ratio of three positive clones closely matched the input ratio, this result suggests that the proposed platform is sensitive enough to discriminate specific binders from nonbinders. 48
Figure 2.23 The number of detected clones per chip in each panning round library. The first and second round panning rounds showed almost same number of positive clones. In the third round panning library, a 140-fold increase from second round panning. The detected positive clones from the fourth round panning library were increased to a 15-fold. 50
Figure 3.1 How to designe “deimmunization” library. To eliminate T-cell epitopes in antibody, mutations to remove T-cell epitopes can generally be used. 53
Figure 3.2 The results of two chip applied for deimminization library. (a) Images of assembled microwell array chips, after overnight incubation(left). Fluorescence images of labeled microwell array(right). Black arrow: cell grown wells, red arrow: fluorescen signal of microwells. (b) In the two chips, 24 clones isolated from each chip and 38 out of 48 clones were successfully isolated. 59

Figure 3.3 The alignment of isolated clones from deimmunization library. Only mutated five sites were shown various. 60
Figure 3.4 The frequency of analyzed clones by NGS. The most frequent clones and second most frequent clones were 1883 and 584, respectively, suggesting that there were repetitively retrieved clones. In the magnified graph, the red bars were positive clones, and black bars were negative clones. The most of the clones that had high counts were the positive. 63
Figure 3.5 The distribution of amino acid in the mutated sites. In the first site, T, N, D accounted for more than 80% of the total, and in the second site, F and Y accounted for more than 70%. In the third site, A occupied almost half the population. In the fourth site, L and I accounted for the vast majority. In the fifth site, I was the most frequent amino acid. 66
Figure 3.6 The proposed platform vs conventional phage display. (a) The proposed platform analyzed 14% of the whole library, but the biopanning method analyzed only 0.01% through 3 round panning. (b) The proposed platform dicovered 112 positive clones, and the conventional method detected only 19 positive clones. Only one clone was detected in both methods. 67

Chapter 1.

Introduction

In this chapter, global market trends for therapeutic antibodies and the conventional technology for antibody library screening will be described. After that, difficulties in the conventional screening method, such as phage display, will be discussed. Finally, the subject of this dissertation, a novel antibody screening method for the detection of rare antibodies by using a high-throughput screening (HTS) platform based on microwell array and automated retrieval system will be presented. This technology reduces panning rounds for minimalizing loss of binders, which has been one of the bottle-neck for the detection of rare antibodies in the conventional phage display method.

1.1. The Therapeutic Antibody Market

1.1.1. Market Trends for therapeutic antibody

Advances in pharmaceutics, molecular biology, and genomics increase the success rate of biologics increased the interest of pharmaceutical companies[1]. The market share of biologics is forecast to rise from 18% to 32% between 2010 and 2024[2]. Especially, antibody drugs have been leading the pharmaceutical market. Sales for antibody drugs have grown from ~$39 billion in 2008 to almost $75 billion in 2013, a 90% increase. In contrast, the salse of other biologics has only increased ~26% at the same time period (Figure 1.1, a). In 2018, antibody drugs were 5 out of the top-10 selling drugs, accounting for 57% of total sales (Figure 1.1, b)[3], and predicted to grow with a CAGR of 12.8% over the next 5~6 years[4]. For this, the requirements of development and commercialization of therapeutic antibodies are increased. In the next section, the development process of the therapeutic antibody will be discussed.

(a)

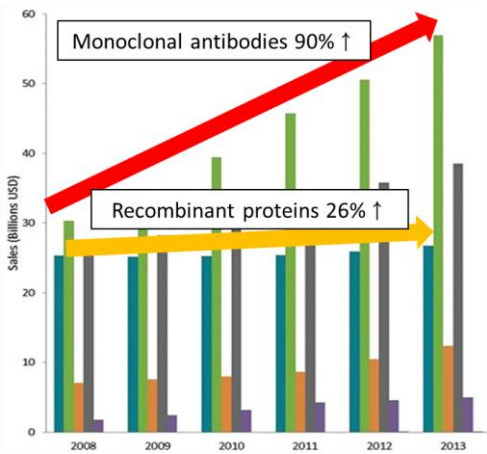

(b)

Rank	Global sales, 2018	Brand (molecule)
1	$20.4bn	Humira (adalimumab)
2	$9.7bn	Revlimid (lenalidomide)
3	$7.6bn	Opdivo (nivolumab)
4	$7.5bn	Enbrel (etanercept)
5	$7.2bn	Herceptin (trastuzumab)
5	$7.2bn	Keytruda (pembrolizumab)
7	$7.1bn	Avastin (bevacizumab)
8	$7.0bn	Rituxan (rituximab)
9	$6.7bn	Eylea (aflibercept)
10	$6.6bn	Xarelto (rivaroxaban)

Figure 1.1 Market trends for therapeutic antibody. (a) Salse of biologics by product type. Note that recombinant proteins were increased ~26% between 2008 and 2013, but monoclonal antibodies were increased ~90% (Reprinted from [2]). (b) Highest-selling drugs in 2018. Five out of the top 10 drugs were antibody drugs (Reprinted from [3]).

1.1.2. The Development Process of Therapeutic Antibody

The process of developing antibody drugs is not much different from that of other drugs. The first step in the drug development process involves target validation and discovery. The difference between chemical drugs and biologics is that biologics require the selection of a production process, such as cell lines. The next step is preclinical testing, which confirms how the drug works and what its safety profile looks like in vitro and in vivo tests. The third step is submitting an Investigational New Drug(IND) application. If the FDA approves IND, then it can move onto human trials. The clinical trial tests the desired effect and side effects on humans and is divided into four stages, including three stages before and one after marketing approval. Once all three stages of the clinical trials are complete, the company files a New Drug Application(NDA). FDA reviews the NDA to determine approval. Research on a new drug continues even after approval[5].

Drug development requires a long time and expensive investment. It takes an average of 13.5 years and $1.78 billion to make one new drug (Figure 1.2), with 0.01% of drug candidates released. From target discovery to commercialization, most candidates will fail during the 'valley of death'. There are two kinds of problems with this valley of death. The enormous timespan and costs that tend to accumulate in the later process, incurred are considerably higher[6], [7].

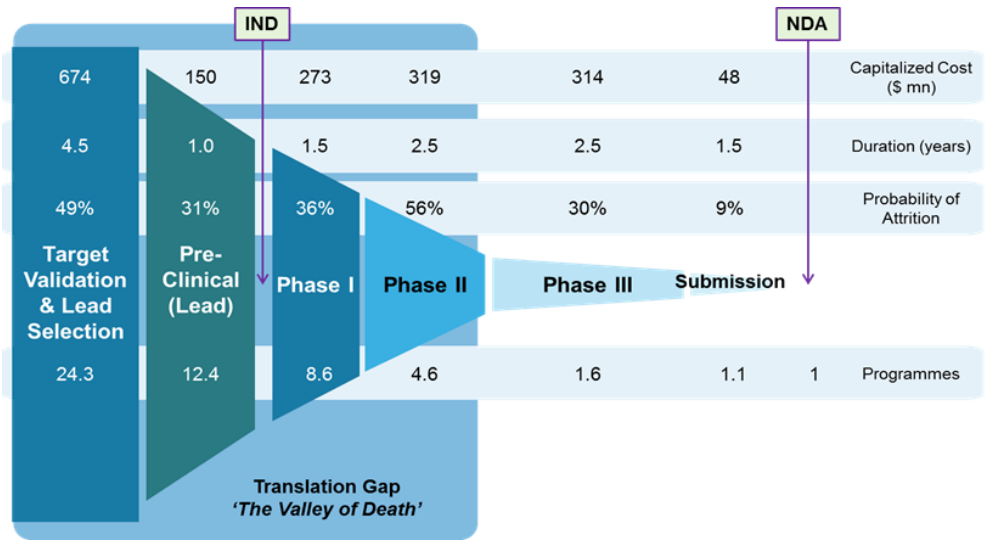

Figure 1.2 Drug-development cycle and the 'valley of death'. Capitalized cost over 13.5 years is $1.8 billion per launch. The cost and time are most consumed in the target validation and lead selection process[6].

It is essential to reduce the failure of the later process by smart lead set in the early stage. Now the question is: How to find smart lead? There is a recent trend for recycling resources to reduce the cost of drug development[8]. Rather than discovering new targets or pathways, technology should be developed to discover the missing leads in existing antibody libraries. Therefore, identification of problems in conventional antibody library screening method is essential.

1.2. Conventional Antibody Library Screening Method

1.2.1. Phage display

The structure of antibody is shown in Figure 1.3. Antibody consists of two light chains and two heavy chains joined to form a Y-shape molecule. The variable region, in the tips of the Y shape, gives specificity for a binding antigen and is divided into complementarity determining regions(CDRs) and frameworks(FRs). CDRs have a high ratio of different amino acids and FRs have more stable amino acids.

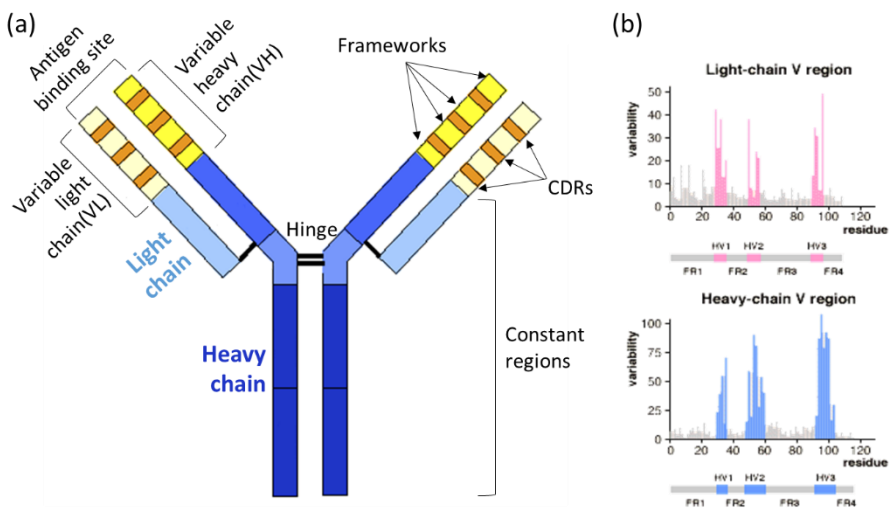

Figure 1.3 Structure of antibody. (a) Composition of antibody[9]. Antibody couples light chains and heavy chains. The variable regions, antigen-binding site, includes the ends of the light and heavy chains. (b) Variability of residues in variable regions. Within light and heavy chains, three CDRs and four FRs exist [10].

The first antibody drug used in humans, Orthoclone (OKT3, Janssen, 1985), was a mouse antibody. However, the use of a mouse monoclonal antibody does not mediate effector functions but stimulates the immune response that induced to neutralize the antibody drug. Mimic human antibodies were developed to avoid immune responses. Chimeric antibodies are hybrid antibodies that combine mouse antigen-binding domains with human constant region domains.

The VH and VL domain gene of the mouse antibody should be obtained to prepare chimeric antibodies. In order to obtain mouse antibodies, mRNA is isolated from spleen B cells of a mouse in which an immune response is induced by injection of a target antigen, and cDNA synthesis based on mRNA. The VH and VL domain genes are obtained by PCR and used as a template of cDNA. cDNA is cloned into a vector such as a phagemid to secure a library. When phagemid libraries containing VH and VL domain genes are inserted into a bacterial host such as E.coli with helper phage, the VH and VL domains are expressed on the surface of phage in a fused form with the geneIII protein of phage. The fused protein is similar to the antigen-binding site of antibody by folding, called scFv(Single chain fragment of variable region)[11].

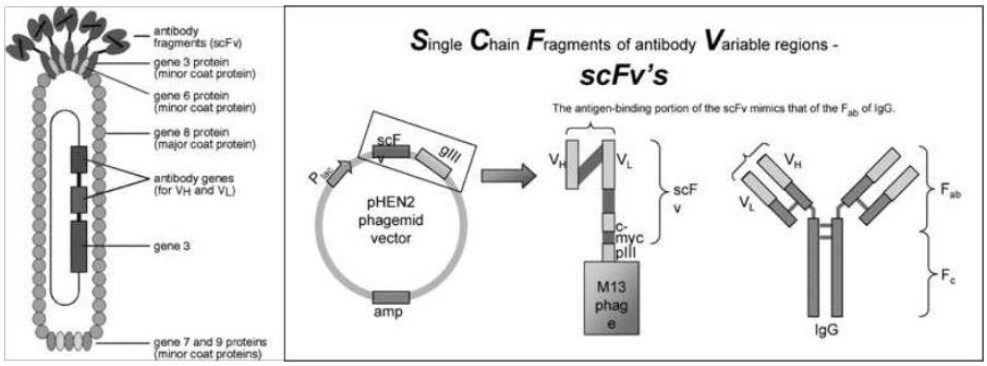

Figure 1.4 scFv structure and DNA recombination in phage display technology. The VH and VL domain are linked to form scFv. scFv is expressed on the surface of phage along with geneIII protein(reprinted from [12]).

The selection of phages expressing the antibody that binds to a target antigen is the phage display technology. In phage display, phages bound antigen are collected and infect E.coli cells to amplify. The amplified phages again bind to the antigen. This process, called the panning process, is repeated multiple rounds. After multiple panning rounds, phage-infected E.coli cells are spread on agar plates for separation to monoclonal antibodies. Phages are rescued from randomly picked colonies and subjected them to Phage ELISA for validation. The antibody DNA sequence is obtained from the selected phage because antibody DNA is encoded into the phagemid[13]. The encoded antibody DNA means that the phenotype and genotype of the antibody can be obtained simultaneously. Maintenance of a genotype-to-phenotype linkage makes the subsequent process easier. Phage display is the most widely used technology for screening antibody

libraries because of its easy amplification and genotype-to-phenotype linkage[14].

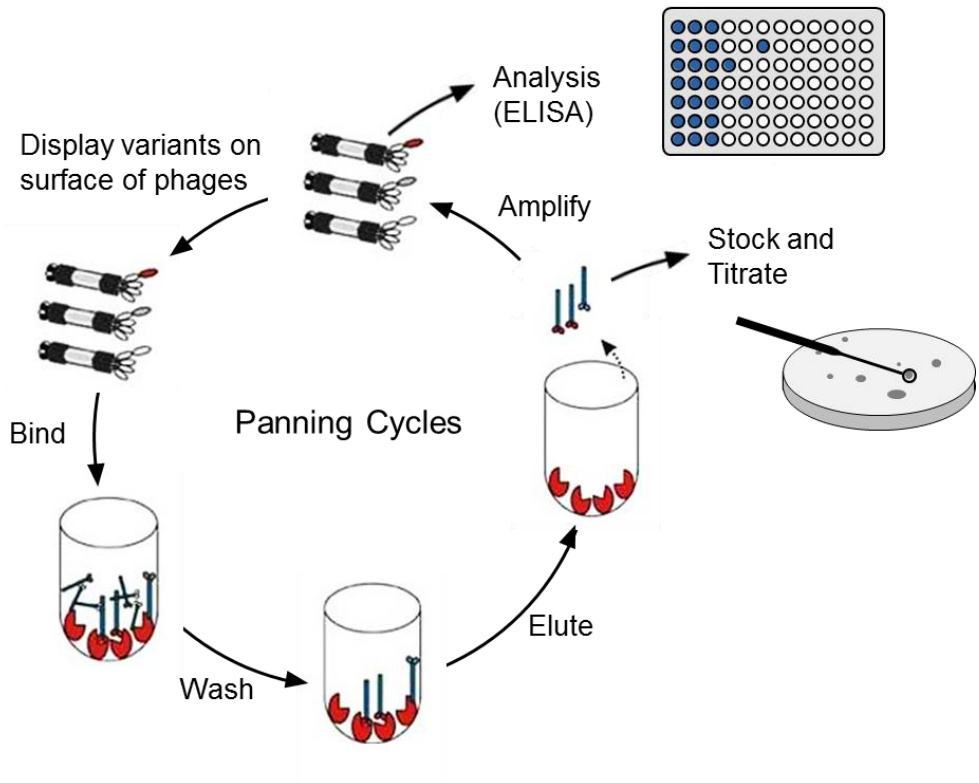

Figure 1.5 The phage display cycle. Specific clones are captured by binding to antigen, and non-specific clones are removed by washing, followed by elution. Phages are amplified by infection and regrowth of phage-producing cells between panning rounds.

1.2.2. Difficulties in conventional phage display

Phage display technology has technical limits, such as limited screening size and loss of binders. First, the capacity of human determines the limits of screening size. The traditional laborious picking and functional testing of individual phages clones limit the screening size to hundreds. Only hundreds of randomly picked clones can be analyzed compared to the size of the whole library(>10^9)[15]. Enrichment of positive clones in the antibody library is required due to this limit. Multiple panning rounds that take from two weeks to a month are consumed for sufficient enrichment.

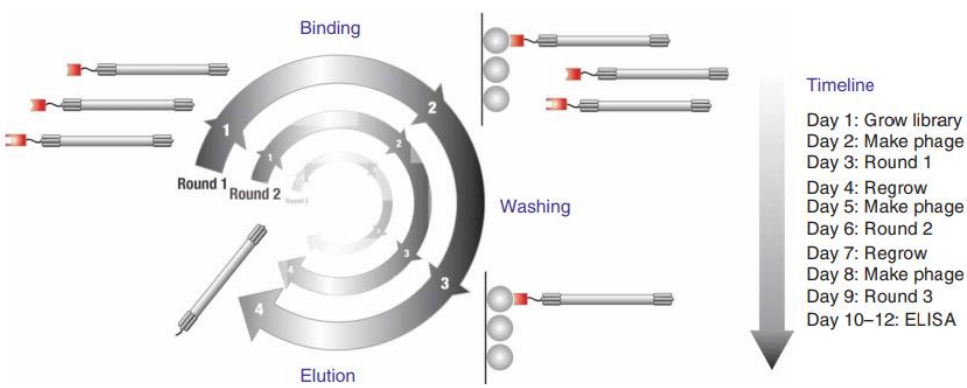

Figure 1.6 Selection of antibody and timeline of phage display. Almost two weeks are consumed for three rounds of panning(Reprinted from [16]).

Besides, it is challenging to obtain the high-affinity binders because its high-affinity interferes with elution. In the elution step, bound phages generally eluted by a change in pH, breaking the binding interactions. If such treatment is not efficient

enough, high-affinity binders will be lost[17].

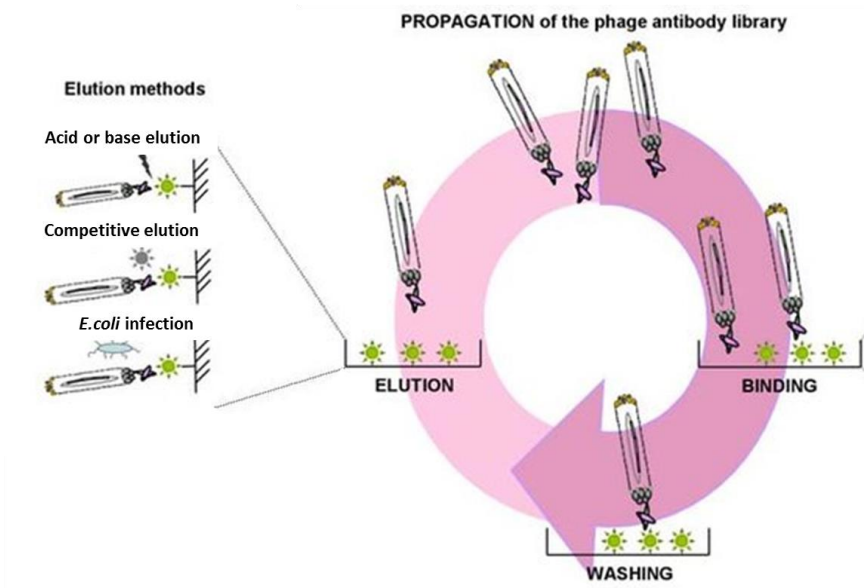

Figure 1.7 Elution methods in panning round. Specific binders to the antigen are released by elution methods. Acid or basic elution is usually used. Competitive elution and directly infecting E. coli method are also used[18].

There is also a loss of rare binders. Dominant clones hide rare binders due to amplification bias in the amplification steps. The amplification step enriches for clones that bind to the desired target antigen. At the same time, the clones that amplified faster are more enriched than other clones with independent characteristics of affinity and growth capacity. Small differences in growth rates of clones lead to bias[19], [20].

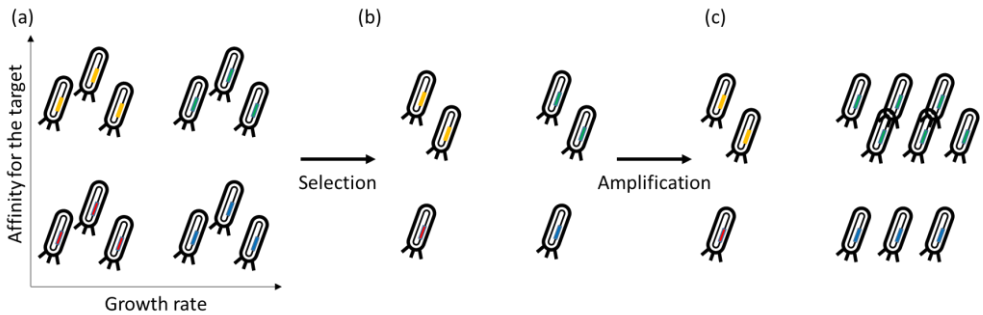

Figure 1.8 The bias in the amplification step. (a) Affinity and growth rate are independent. (b) Phages that bind to the specific antigen are selected, and non-specific binders are also selected. (c) The amplification step further enriches clones that have a growth advantage.

Multiple panning rounds are essential to enrich positive clones in a phage library because only hundreds of clones can be handled. The loss of binders become worse during multiple panning rounds. The use of high-throughput methods can reduce the number of panning rounds to minimalize laborious work and the loss of binders, which increases chances to obtain undiscovered clones. In the next section, the high-throughput methods that have been applied to different steps of phage display technology will be described.

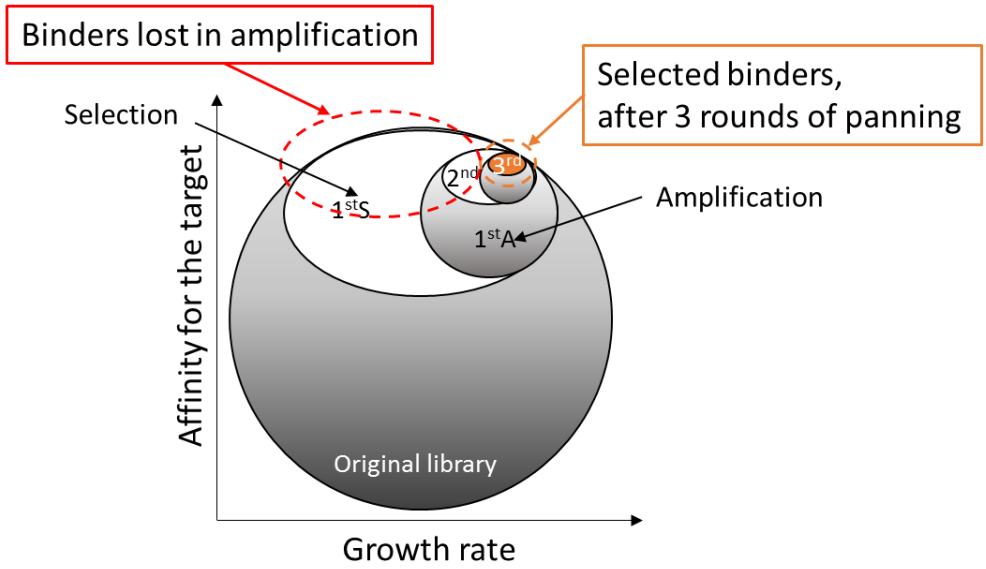

Figure 1.9 Diagram of changes in the size of library during three rounds of panning. After three rounds of panning, the screen identifies binders. The number of identified binders, however, is much smaller than the number of binders that were originally present in the library..

1.2.3. Previous researches on phage display technology applied the high-throughput methods from other

The panning round of phage display involves four processes, including binding, washing, elution, and amplification. Multiple panning rounds are required for enrichment of positive clones in the antibody library because only hundreds of randomly picked clones can be analyzed. However, multiple panning rounds cause time-consuming, laborious work, and the loss of binders.

Phage display has been advanced in different steps. The use of magnetic beads increases the throughput and efficiency of the phage binding step[21]–[24]. Automated procedures for reducing laborious work in colony selection and phage-ELISA allow the simple handling of multiple samples in parallel with a multichannel pipetting device and 96well plate[24]–[26]. However, these methods do not eliminate the need for multiple panning rounds and colony picking to identify single clones[27].

Microtechnologies have been applied to phage display for reducing the number of panning rounds. The miniaturization of a reaction chamber, a hallmark of microtechnology, increases throughput that allows hundreds of thousands of clones to screen at once. The microcapillary array method offers densely packed arrays and an automated air retrieval system for multiplexed capacities[28]. However, the retrieval system is assumed to be inefficient in that pneumatic pressure is not sufficient to isolate the sample by a small target spot and capillary force.

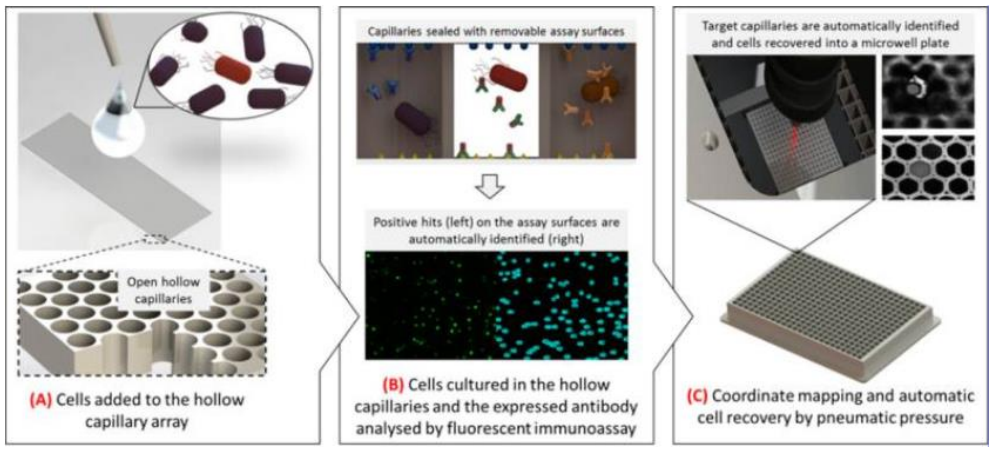

Figure 1.10 Schematic of the microcapillary method. Single cells are captured in densely packed microcapillary arrays and sealed. Target capillaries are automatically identified, and cells are recovered by the pneumatic pressure(reprinted from [28]).

The micro-emulsion method utilizes water-in-oil emulsions containing antigen-coated magnetic beads, and Fluorescence Activated Cell Sorting (FACS) By using the FACS machine to sort beads containing phages, the number of panning rounds is reduced, and the need for colony picking is eliminated in a high-throughput manner[27], [29]. However, cross-contamination between the beads may occur. The beads are collected into single space following the breakage of droplets, which is continued until the beads are separated into individual spaces using the FACS machine. Since all beads gathered in single space, the phage bound to the bead may be detached and bind to the other bead[30]. Therefore, the application of microtechnology to phage display, which can significantly increase throughput to decrease panning rounds, remains an unresolved problem.

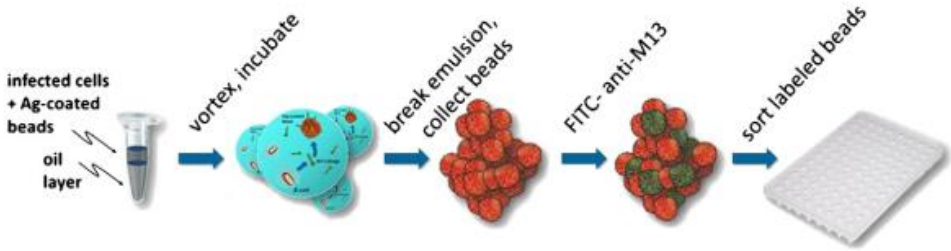

Figure 1.11 Diagram of the micro-emulsion method. Cells are compartmentalized with antigen-coated beads in a water-in-oil emulsion. The emulsion is broken, and the beads are collected. The labeled beads can be sorted by flow cytometry(reprinted from [27]).

1.3. Main Concept: a technology for high-throughput phage display using a microwell array chip and automated retrieval system

The main theme of this dissertation is the acquirement of undetected clones by reducing panning rounds using a high-throughput phage display method. Figure 1.12 shows the schematic illustration of the concept. The high-throughput phage display method can be generated by the microwell array chip and automated laser retrieval system[31], [32]. The microwell array chip isolates single-cell into each sealed space to prevent cross-contamination. After an adequate amount of secreted phages bind to the antigen that coated inside the well, non-specific binders are washed. Using a fluorescence reporter, remained phages are detected. The detected phages are recovered by an automated laser retrieval system, and NGS analyzes the encoded antibody sequence in phagemid.

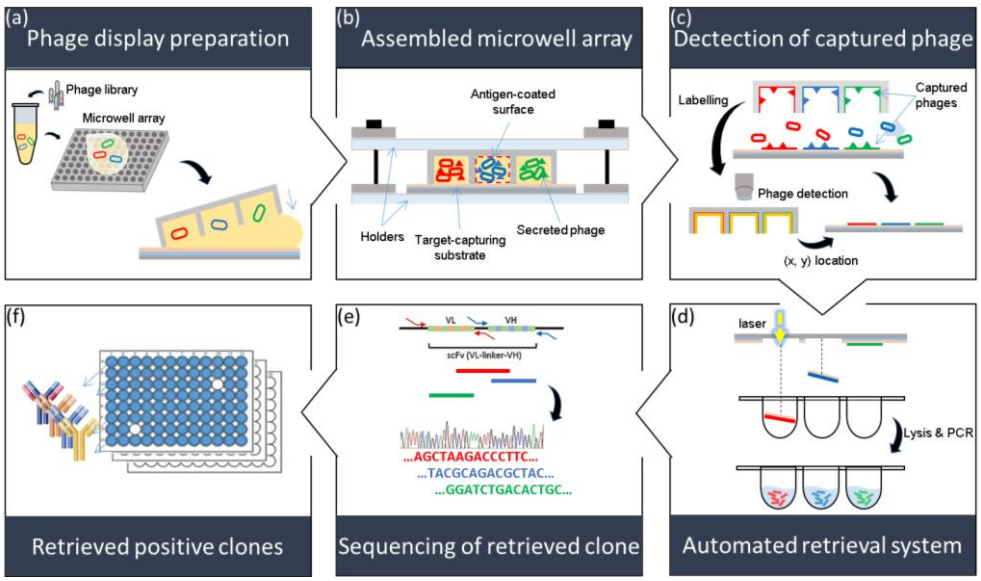

Figure 1.12 Main concept of proposed technology: A high-throughput phage display using a microwell array chip and automated laser retrieval system. (a) Phage-infected cells added to the microwell array. (b) The microwell array was mounted on the chip holders with the target-capturing substrate in order to isolate individual microwells. Phages were secreted from cells and captured. (c) After overnight incubation, the microwell array chip was disassembled. Cells and non-specific binders were removed, and captured phages on the microwell array were labeled. The position information of captured phage on the microwell array was transferred to the target-capturing substrate. (d) The obtained positions of the target samples were retrieved by using the automated laser retrieval system. Retrieved phages were lysed, and encoded antibody sequences were amplified by PCR. (e) High-throughput sequencing was performed by using TrueRepertoire^{TM}(Celemics)[33]. (d) For

validation of retrieved phages, phage-ELISA was performed.

1.3.1. My Works in This Dissertation

I thought that the PDMS(polydimethylsiloxane)-microwell array was more potential because of its high accessibility and easy fabrication, and the automated isolation system using the pulse laser was more suitable to maximize the retrieval efficiency. If the insufficient performance of the retrieval system in other technologies can be improved, then it would be more appropriate to a high-throughput phage display for eliminating the panning rounds. For the high-throughput phage display, the list of limitations of previous technologies, and the proposed solutions in this dissertation to resolve them are as follows.

(1) The holder maintining assembled microwell array chip needs to be developed. PDMS-microwell array should be laid onto the glass slide for sealing individual microwells. Holder clamps the assembly of the microwell array and glass slide. The holder reduces cross-contamination between microwells during incubation. I developed a hybrid holder that combined the acryl sheet and aluminum plate to avoid deformation.

(2) The concentration of loaded cells should be diluted to a specific concentration for the prevention of occupying multiple cells in one well. In order to achieve this condition, the input concentration of cells, and the output concentration of cells should be linear. To determine the single-cell loading condition, I performed statistical analysis with tests of various

concentrations of cell solution.

(3) The microwell array chip for phage detection and retrieval needs to be developed. The microwell array chip is consists of a microwell array, glass slide, and holder. Independent substrates for detection and phage retrieval are advantageous in preventing cross-contamination. The pattern of well structures also allows for easier detection in the microwell array. I developed systems separated by detection and retrieval, which can support a clear in-well image and prevention of cross-contamination

(4) The additional layer is needed to minimize the loss of retrieved phages. Laser-induced sample isolation has been developed in recent years[34]. The sacrificial layer is required for laser energy absorption. However, this method can be used to transfer a single morphology sample, such as a cell, but not suitable for transferring multiple small molecules such as phages at once. Because the substrate on which the phages are captured vaporizes and disappears, molecules can be scattered sporadically. I developed the additional layer deposited on the sacrificial layer for efficient phage recovery without loss and damage of retrieved phages.

The outline of this dissertation is as follows. In chapter 2, the developmental process and validation of the proposed technology will be described by dividing it into five steps, as shown above. In chapter 3, the application for the screening of the de-immunization library will be demonstrated. Finally, in chapter 4, I will discuss the meaning of the proposed technology and the potential impact of my works.

Chapter 2.

System Development

In this chapter, the entire developmental process and validation are divided mainly into five parts. (1) How to prepare phage display and microwell array chip? I developed a PDMS-microwell array and hybrid holder. This section will describe the concept and quantitative analysis of the cell culture in the microwell array chip. (2) How to detect target samples? I developed independent substrates for detection and retrieval and automated image analysis. (3) How to retrieve target samples? I developed the target-capturing substrate that can prevent the loss of target samples. (4) How to analyze retrieved clones? I will describe the sequencing method and the Phage-ELISA method that I have tried. (5) How to validate the proposed technology? This section will present the results of the test for the various combination ratio of positive clone and negative clone for validation.

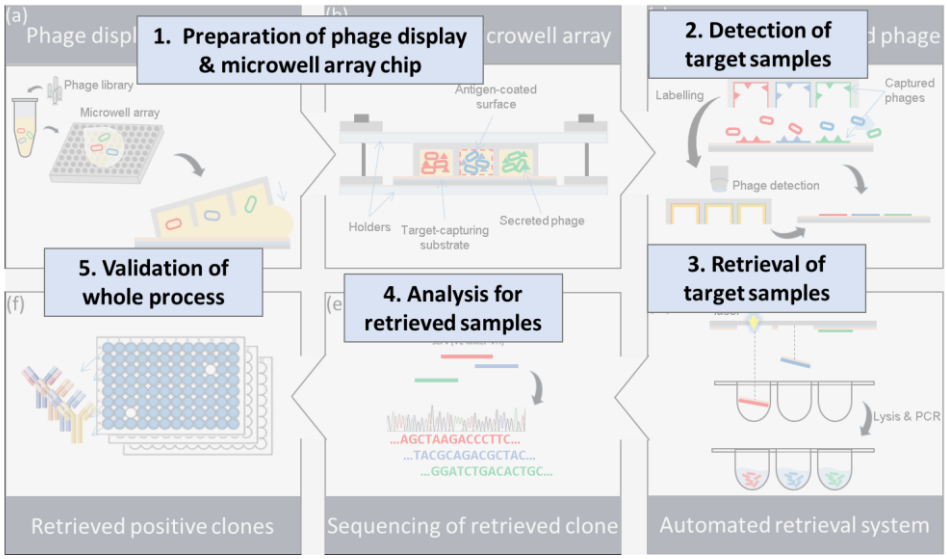

Figure 2.1 System Overview. In chapter 2, the entire development process of the proposed technology will be described by dividing it into five parts. (1) How to prepare phage display and microwell array chip? (2) How to detect target samples? (3) How to retrieve target samples? (4) How to analyze retrieved clones? (5) How to validate the proposed technology? will be described.

2.1. Preparation of phage display and microwell array chip

2.1.1. PDMS microwell array for long-time cell culturing

The PDMS was decided to the material of microwell array, which is more potent because of its high accessibility and easy fabrication. The microwell array was fabricated using soft-lithography in which polydimethylsiloxane (PDMS, SYLGARD 184, Dow Corning) was cast onto a silicon mold having SU-8 photoresist pattern (SU-8 2015, Microchem) and cured for 30 minutes at 120℃ [35]. The cured 3mm-thick PDMS block having a two-dimensional array of microwells was obtained by peeling off from the mold.

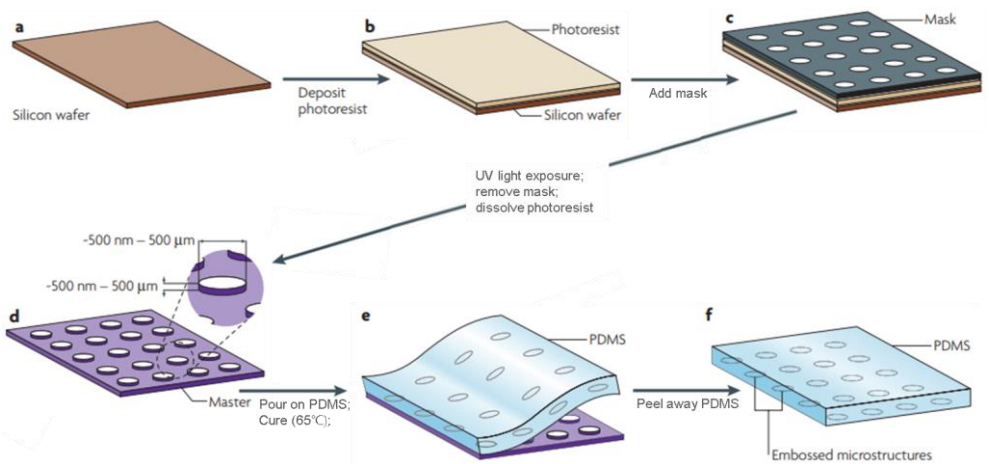

Figure 2.2 The fabrication of micropatterend slabs of PDMS. (a, b) The photoresist is spin-coated on a silicon wafer. (c) A mask is placed in contact with the layer of photoresist. (d) The photoresist is illuminated with ultraviolet (UV) light through the mask. An organic solvent dissolves and removes photoresist that is not crosslinked. (e) PDMS is poured on the master, cured thermally, and peeled away. (f) The

resulting layer of PDMS has microstructures embossed in its surface (reprinted from [35]).

The smaller the microwell size, the higher the capacity of the array, but enough space is required for the occupied cell to grow during the incubation. The smallest microwell size in which a single-cell incubation should be used. Experiments with different well sizes showed that a well size of d 60μm and h 40μm was the most suitable. The size of the microwell array is designed to fit the glass slide size for compatibility with the instruments. The microwell array is consists of 113,000 wells and largely divided into 200 blocks of 20 x 10, with one block of 27 x 21 microwells(Figure 2.3). Each block had position markers (x, y). Bacteria expressing GFP and RFP, respectively, were loaded and incubated to verify that the designed microwell array was suitable for cell growth during overnight incubation. The culture results are shown in Figure 2.4. During 19 hours of incubation, occupied cells were grown sufficiently.

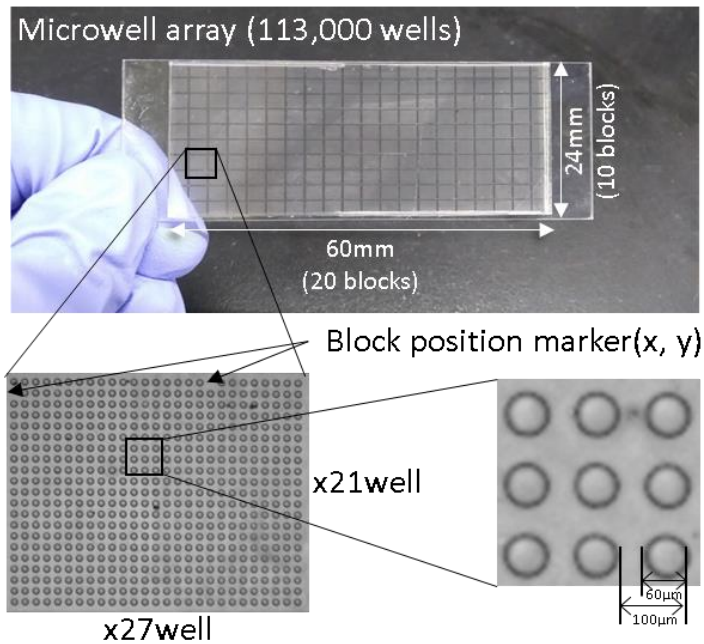

Figure 2.3 The bright field images show PDMS microwell array. The microwell array was consists of 113,000 wells and largely divided into 200 blocks of 20 x 10, with one block of 27 x 21 microwells(d 60μm, h 40μm). Each block had position markers (x, y).

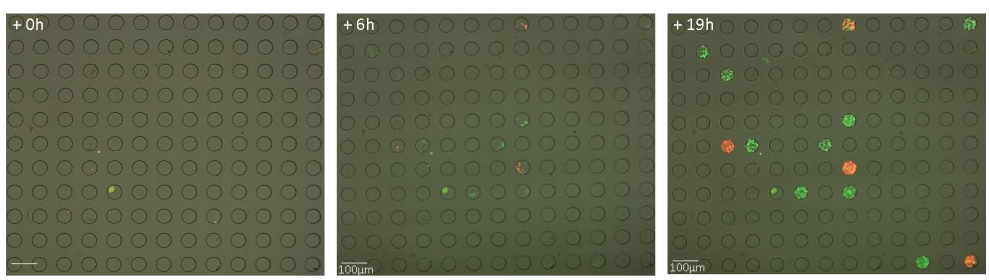

Figure 2.4 The fluorescence images show that occupied cells were grown sufficiently during 19 hours of incubation. Bacteria expressing GFP and RFP, respectively, were

loaded and incubated.

2.1.2. The single-cell loading condition in the microwell

The concentration of loaded cells should be diluted to a specific concentration for the prevention of occupying multiple cells in one well. When calculated according to the Poisson distribution, 95% of occupied wells are under the single-cell condition that is satisfied if 10% of the entire well array is filled by the cell (Figure 2.5). In order to achieve this condition, the input concentration of cells, and the output concentration of cells should be linear. If it is not linear, it will not be able to meet single-cell conditions uniformly. The various concentrations of cells were applied to microwell arrays. The average number of cells in one well, which calculated from the ratio of occupied wells and empty wells by the Poisson distribution, and the input concentration of cells were compared. When the input concentrations of cells were OD 0.92, 0.52, 0.1, 0.05, 0.02, on average 1.78, 1.05, 0.23, 0.16, 0.1 cells entered one well (Figure 2.6). This result shows that the input concentration of cells and the output concentration of cells had a linear proportional relation. When an input concentration of cells was OD 0.02, 10% of the wells were occupied by the cell, thereby obtaining a single-cell condition to be applied in the following experiments.

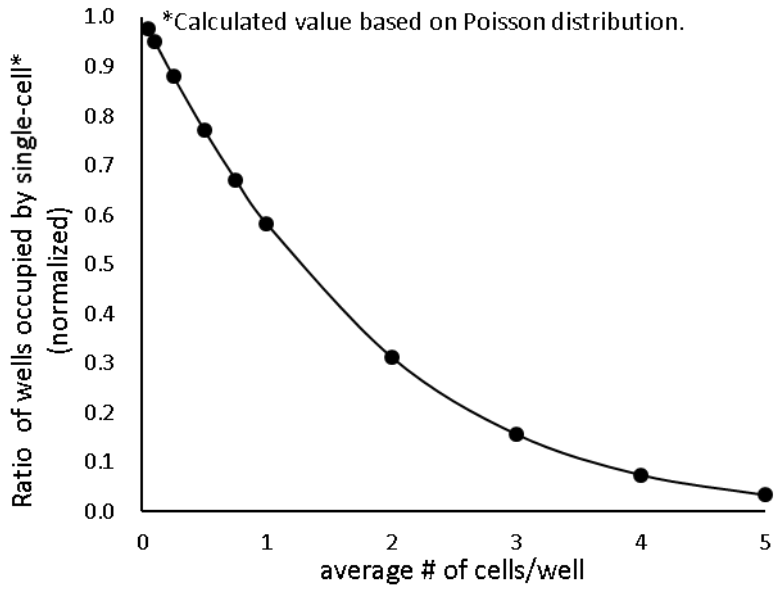

Figure 2.5 The average number of cells in one well and the ratio of wells occupied by single-cell based on Poisson distribution. When the average of 0.1 cells was entered in one well, 95% of occupied wells are under the single-cell.

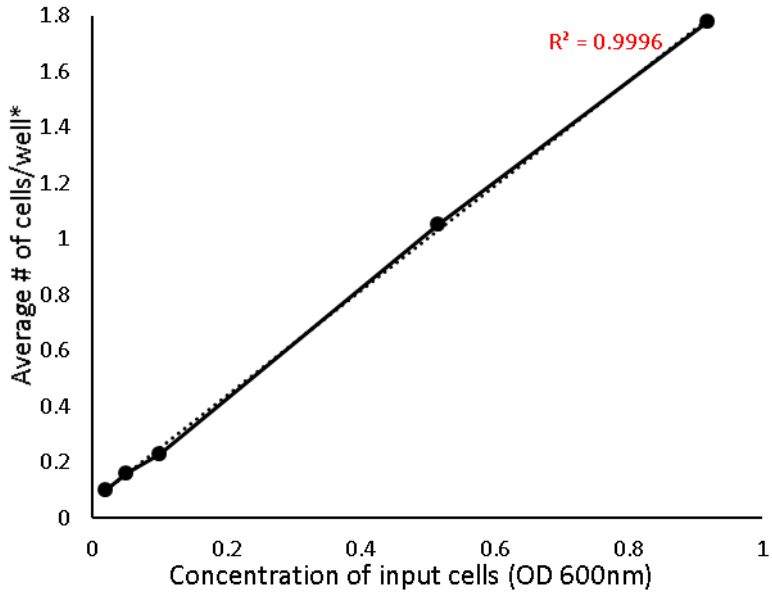

Figure 2.6 The input concentration of cells and the average number of trapped cells/well based on Poisson distribution. The average number of trapped cells/well was calculated according to the Poisson distibution based on the ratio of wells occupied by the cells in the total chips. Input concentration of cells and the output concentration of cells had a linear relation. If the input concentration of cells was 0.02, the average of 0.1cells could be entered in one well(10% of the wells occupied) that fulfill a single-cell condition.

2.1.3. Design of holder by a hybrid structure

Right after loading of cells, the microwell array was mounted on the chip holder with the sample-capturing substrate. The microwell array and the sample-capturing substrate were directed to each other for sealing individual microwells. Holder clamps the assembly of the microwell array and sample-capturing substrate to prevent cross-contamination. The holder maintaining assembled microwell array chip was required. For image processing, the holder must be transparent or window structure. First, a window-type aluminum plate was designed as a holder. However, the deformation of the microwell array caused by the window structure during overnight incubation. The deformation prompted the cross-contamination of the cell out of the well(Figure 2.7).

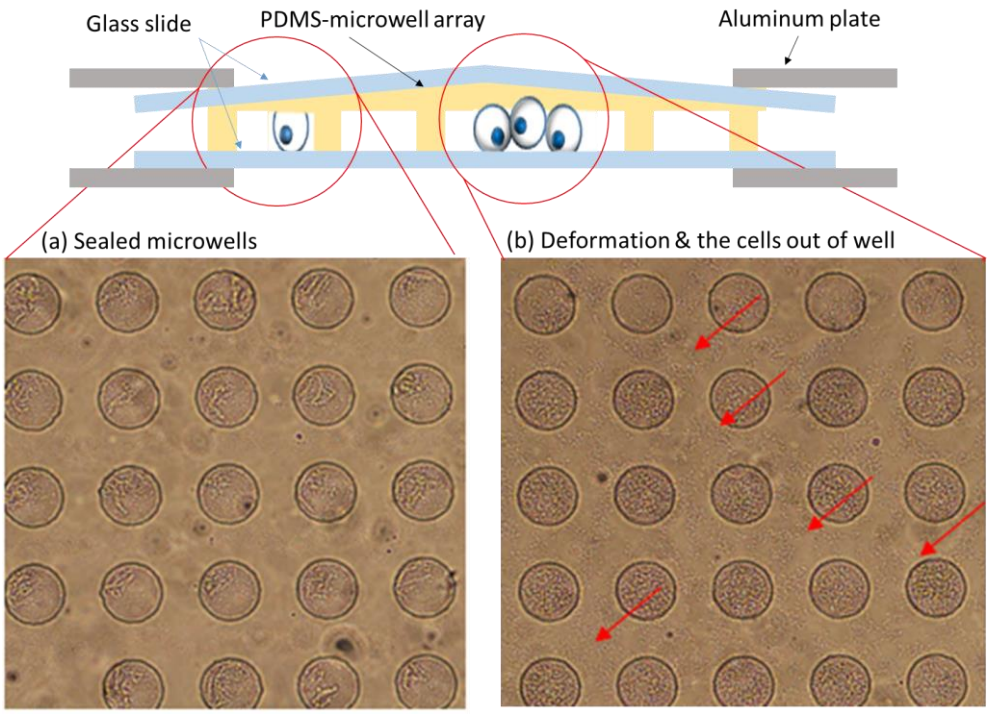

Figure 2.7 The deformation of the microwell array chip in the window-type aluminum plate holder. (a) Perfectly sealed microwells. (b) Deformation of microwell array and the cells out of well.

A holer made of 5mm thick acryl sheet was also designed to inhibit deformation, but the same problem occurred. A hybrid holder structure was lastly designed that combined the acryl sheet and aluminum plate (Figure 2.8). This hybrid holder did not show deformation, a problem other previous holders had. The chip holder was designed to fit into conventional microplate reader format and allow optical imaging through a transparent window while maintaining reliable compartmentalization of individual microreaction chambers by tightening screws.

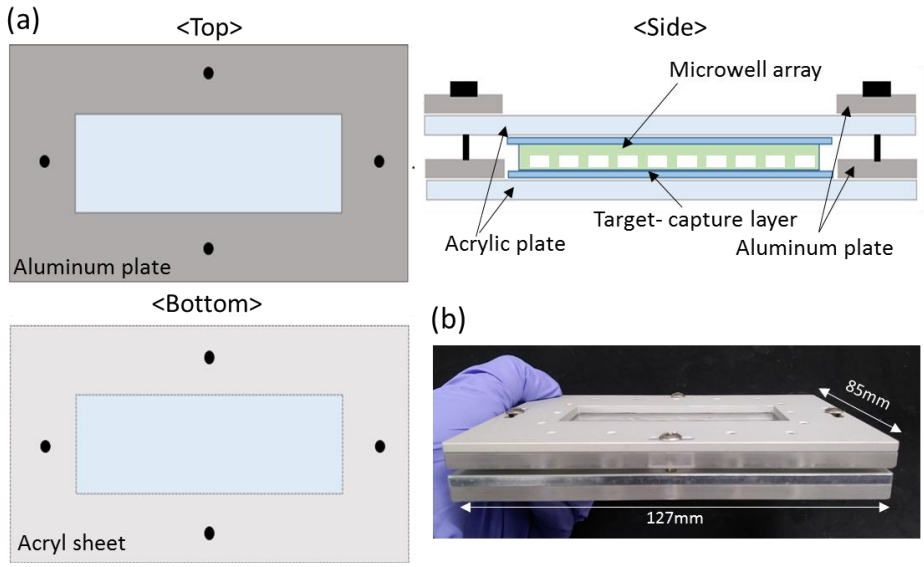

Figure 2.8 The structure of the hybrid holder. (a) Schematic representation of the holder. (b) Image of the holder. The holder consisted of an aluminum plate and an acryl sheet and was designed to a size of 96well plate.

2.2. Detection of target samples

2.2.1. Independent substrates for detection and retrieval

After overnight incubation, the microwell array chip was disassembled back to the microwell array and the target-capturing substrate. Independent substrates for detection and phage retrieval are advantageous in preventing cross-contamination. The pattern of well structures also allows for easier detection in the microwell array. At the same time, the target-capturing substrate was deposited on the sacrificial layer that vaporized by energy absorption to isolated target samples. About the target-capturing substrate and retrieval system will be described in chapter 2.3. Fluorescence reporters labeled surface-bound phages in the microwell array. The labeled microwell array was washed, re-assembled with a non-treated glass slide, and mounted to the holder for subsequent imaging. The (x, y, z) coordinates of the target sample obtained after image analysis were converted into the target sample positions on the sample-capturing substrate.

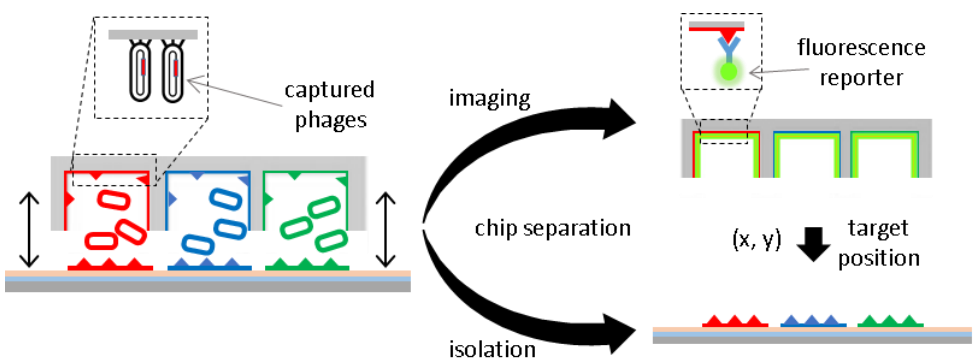

Figure 2.9 The independent process of microwell array and sample-capturing

substrate. The microwell array was used for target imagning and the sample-capturing substrate was used to isolate target samples. The target positions analyzed from microwell array images were applied to sample-capturing.

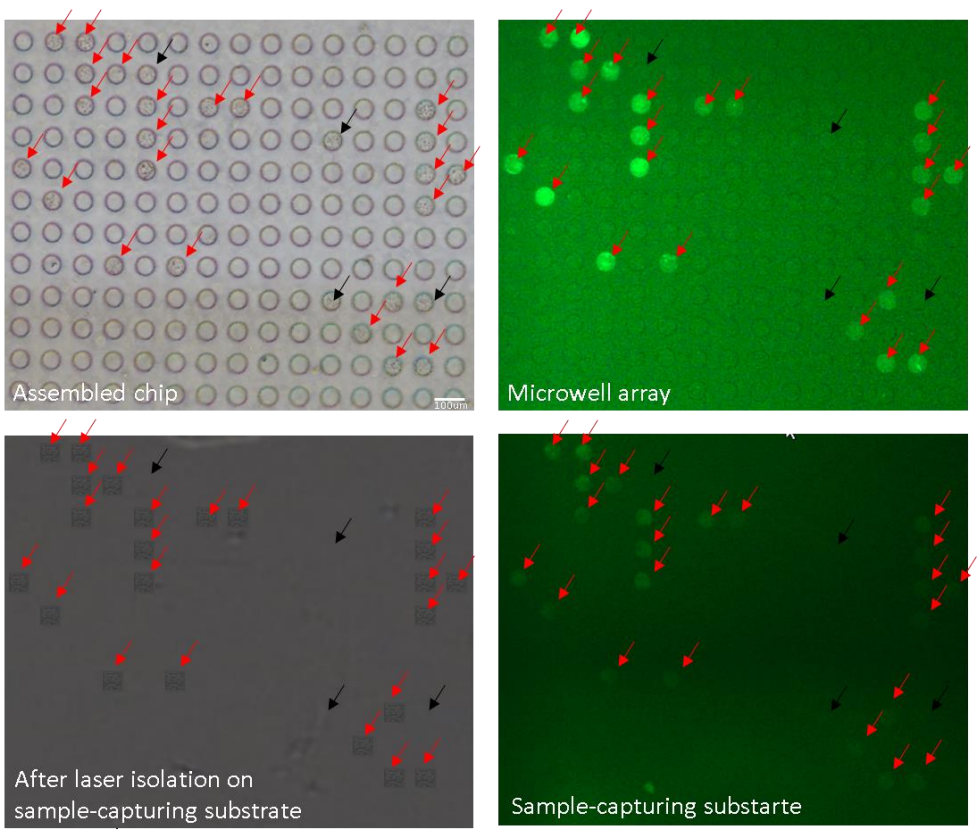

Figure 2.10 The bright-field image of the assembled microwell array chip. After labeling, the fluorescence images of the microwell array and sample-capturing substrate, and isolated surface of sample-capturing substarte.(Black arrow: well occupied by cells with no fluorescence signal, red arrow: well occupied by cells with fluorescence signal)

2.2.2. Automated imaging process

Brightfield and fluorescence images of the microwell array chip were acquired by using an automated fluorescence microscope equipped with a high-sensitivity charge-coupled device camera. The image acquisition process was performed before and after the disassembly of the microwell array chip, respectively. The acquired individual images were stitched into a large reconstructed image showing the whole microwell area of a single microwell array chip[36].

In order to provide the positions of target samples to be retrieved from the chip, a Python script for image analysis was developed and utilized. To be more specific, coordinates of individual microwells and the corresponding fluorescence intensities were firstly extracted from the stitched images. By comparing the coordinates of the microwells and on-chip alignment markers obtained before and after the chip disassembly, target sample positions on the sample-capturing substrate were then determined(Figure 2.11). The obtained positions of the target samples were finally converted into the form of the displacements needed for the operation of a laser-based sample retrieval system. Every interface was developed by GUI for user-friendly (Figure 2.12).

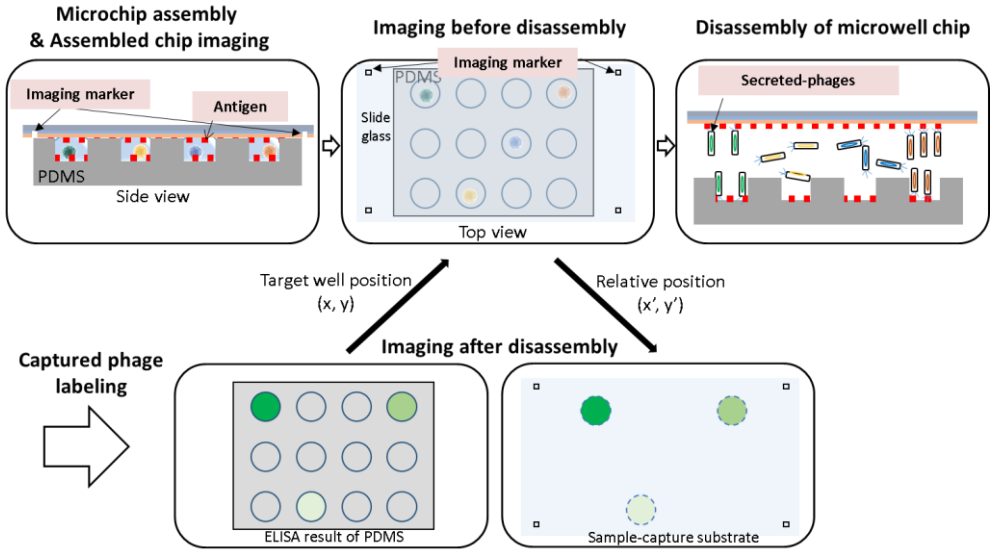

Figure 2.11 Schematic of deriving target position. The image acquisition process was performed before and after the disassembly of the microwell array chip, respectively. The target well position (x, y) was obtained from labeled microwell array. Relative position was derived from image of assembled chip.

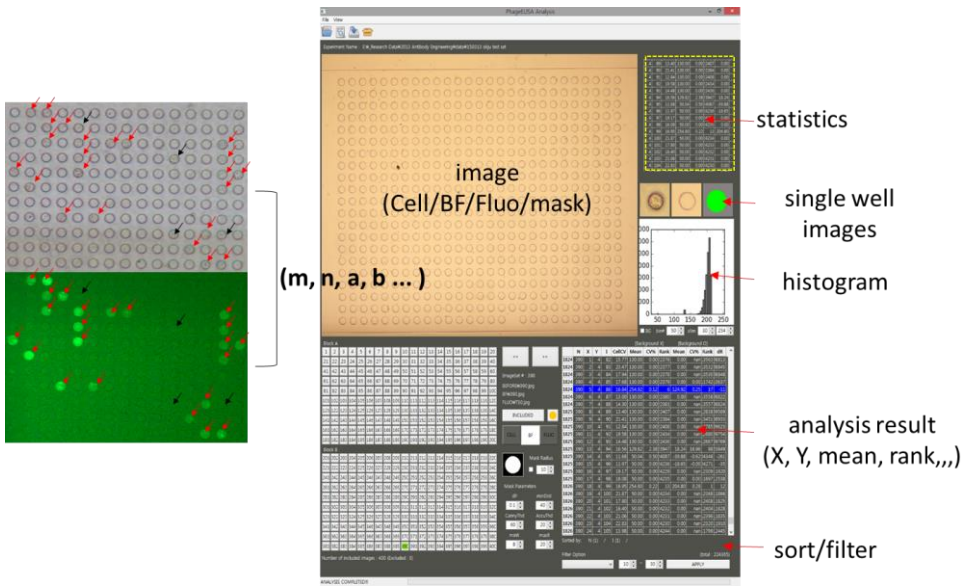

Figure 2.12 GUI program for obtaining target position on labeled microwell array and relative position from assembled microwell array chip.

2.3. Retrieval of target samples

2.3.1. The phage capturing layer for retrieval using laser

There were many changes in chip design before the current chip structure was determined, based on a microwell array chip and laser system. First, a PS plate such as an ELISA assay plate was used as the sample-capture layer. The petri dish was cut into the size of a glass slide and the antigen was coated on the hydrophilic PS surface to obtain a clear image (Figure 2.13). However, the phage could not be separated from the PS substrate by laser and was recovered by cutting the PS plate by hand. The ease of recovery of captured phage and keeping PS substrate were considered to

design the next chip structure.

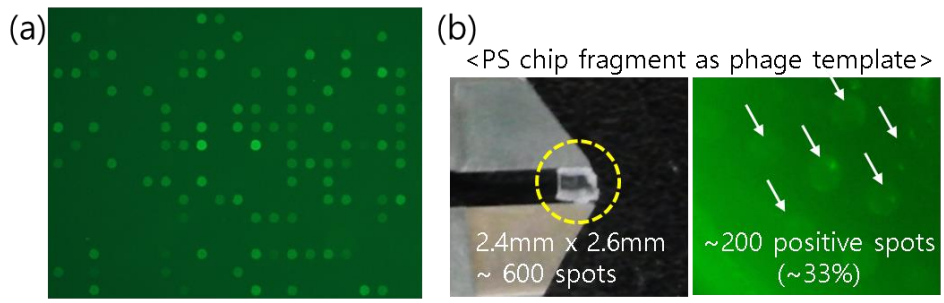

Figure 2.13 (a) Fluorescence image of PS substrate. (b) PS fragment for phage retrieval, about 600 spots in the 2.4mm x 2.6mm area. Among them, 200 spots were positive clones.

The method that creates a PS pallet in the microwell and simultaneously performs target imaging and recovery from the microwells was developed [37] (Figure 2.14) because of the characteristics of PS that easy fabrication and no-autofluorescence. The microwell array was immersed in the PS solution and then slowly withdrawn to isolate PS solution in each well. Evaporation of solvent resulted in a concave PS pallet inside each well. This method had the advantage of easy retrieval, but due to the deformation of the PDMS during incubation by PS pallet, a gap was generated between the pallet and the microwell, which leads to cells and phages catching in the gap. Cells and phages in the gaps caused a lot of noise in the image and contamination in the recovery step (Figure 2.15).

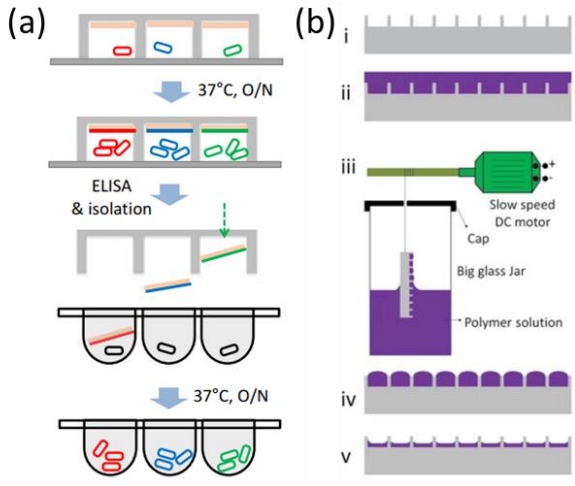

Figure 2.14 Schematic of the PS pallet in microwell model. (a) The microwell array containing PS pallets performs target imaging and recovery from the microwells. (b) Scheamtic of the fabrication process. (i) A PDMS microwell array (shown in gray) is fabricated by a standard molding process. (ii) A polymer solution (shown in purple) is added to the PDMS microwell array. (iii) The wetted PDMS mold is immersed in the polymer solution and then slowly withdrawn. (iv) The dewetting of polymer solution from PDMS results in isolated convex polymer solution in each well. (v) Evaporation of solvent results in concave polymer microrafts inside each well(reprinted from [37])

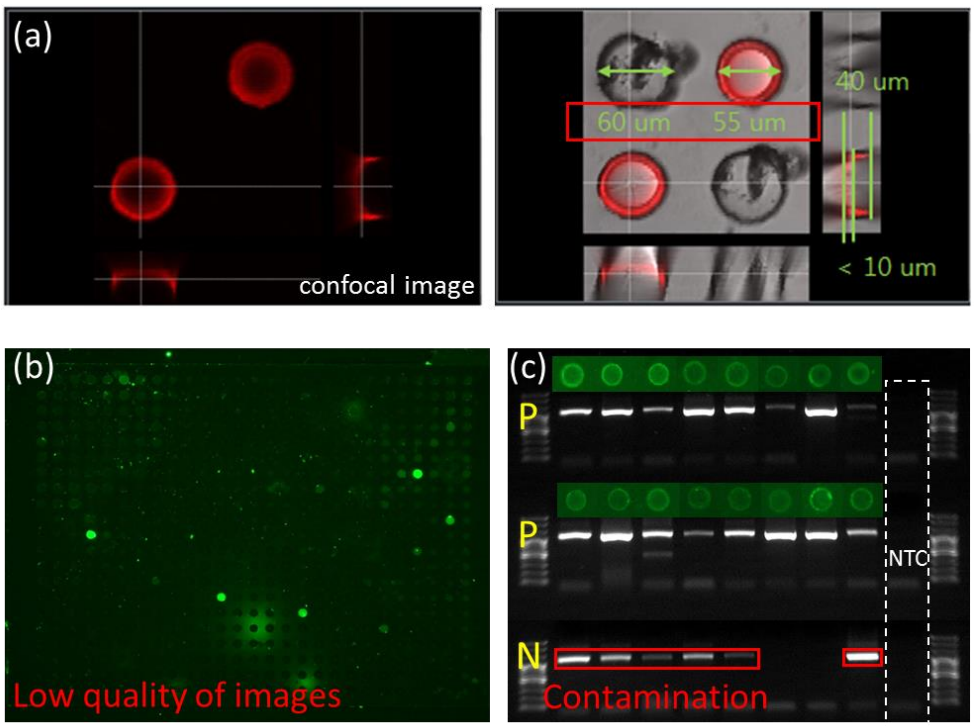

Figure 2.15 The results of the PS pallet model. (a) Confocal imaged of the PS pallet. The deformation of micowell was caused by PS pallet. (b) Fluorescence image of labeled microwell array containing the PS pallet. The quality of image was low because of the gap between microwell and PS pallet. (c) The results of pallet retreival method using gel electrophoresis. There were contaminzation during the sample retrieval.

The next method was to mix low-melting agarose with a suspension of cells, which were present as a liquid during incubation(37℃), and then solidified in a refrigerator after overnight incubation to produce agarose pallet or pillar. The pallet

that remained in the microwell was not isolated by laser, but when the pallet was transferred to the sample-capture substrate to form a pillar, it was easily isolated. The agarose residue in the microwell did not wash, which induced false-positive. As shown in figure 2.16, negative clones were detected as positive clones.

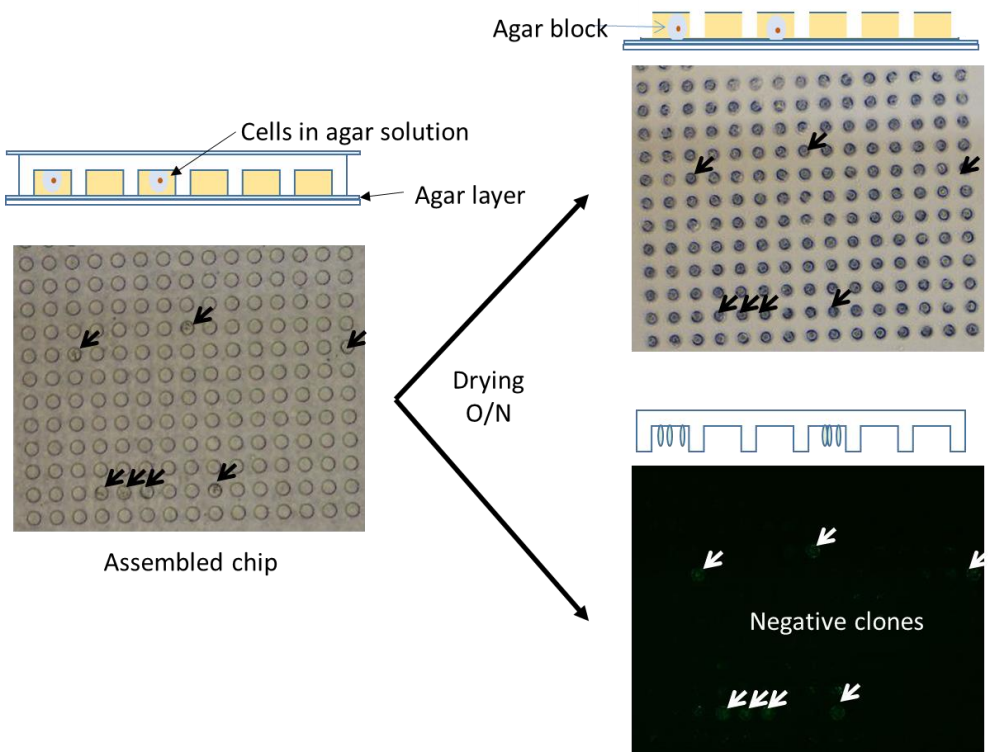

Figure 2.16 The before and after images of disassembled microwell array in agarose pillar model. After overnight drying, agarose pallets were transferred to sample-capturing substrate. Because of residual agarose in microwell array, false positive was detected.

Finally, the method of depositing the sample-capturing layer on the sacrificial layer was developed. The sacrificial layer absorbed the layer energy and vaporated to punch the sample-capturing layer that prevents dispersing captured phages (Figure 2.17). The sample-capture layer which was fabricated using SU-8 and PDMS affected areas other than the laser targeted area, causing the sample-capture layer to lift or tear. If the layer was more crackable than SU-8 or PDMS, it would be easier to isolate using a laser. The crack-prone material, h-PDMS(hard-polydimethylsiloxane) was selected. The h-PDMS that fabricated by thermal curing, has shorter cross-linkers and lower elongation at break as compared to those in the PDMS[38], [39].

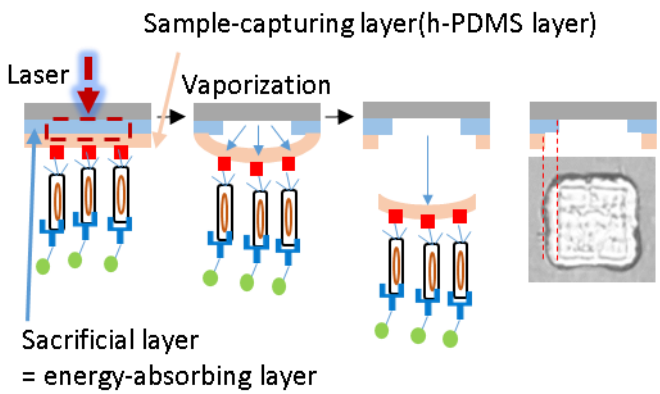

Figure 2.17 Schematic of isolation process. The sacrificial layer absorbed the layer energy and vaporated to punch the sample-capturing substrate.

2.3.2. The automated laser-driven sample retrieval system

The sample retrieval system developed in our group [32] was utilized under the control of a Python script written for this work. Briefly, the retrieval system comprised two motorized stages, a CCD camera, light source, laser source, pulse slit, objective lenses. The two motorized stages could be controlled automatically by communicating with a computer. One was for loading sample slides, and the other was for loading tubes to receive isolated phages. The CCD camera was installed to observe where the laser pulse would be applied through the objective lenses. A slit is located in the light path between the laser source and the objective lens to control the region to be isolated. The slit is controlled either manually or automatically to adjust the size of the laser pulse.

Two independent 3-axis mechanical stages and an infrared pulse laser were operated in a synchronized manner in order to selectively separate phage of interest from the surface of the target-capturing substrate. The sacrificial layer(ITO) was coated on a glass side by sputter deposition, and then the target-capturing layer(h-PDMS) was deposited. An infrared laser was applied to the target area, vaporizing the ITO layer and punching the target-capturing layer. The retrieved phages were collected in an 8-strip PCR tube filled with phage lysis buffer for lysis of phage coat protein. scFv region in phage viral DNA was then amplified using PCR and sequenced by the Sanger method.

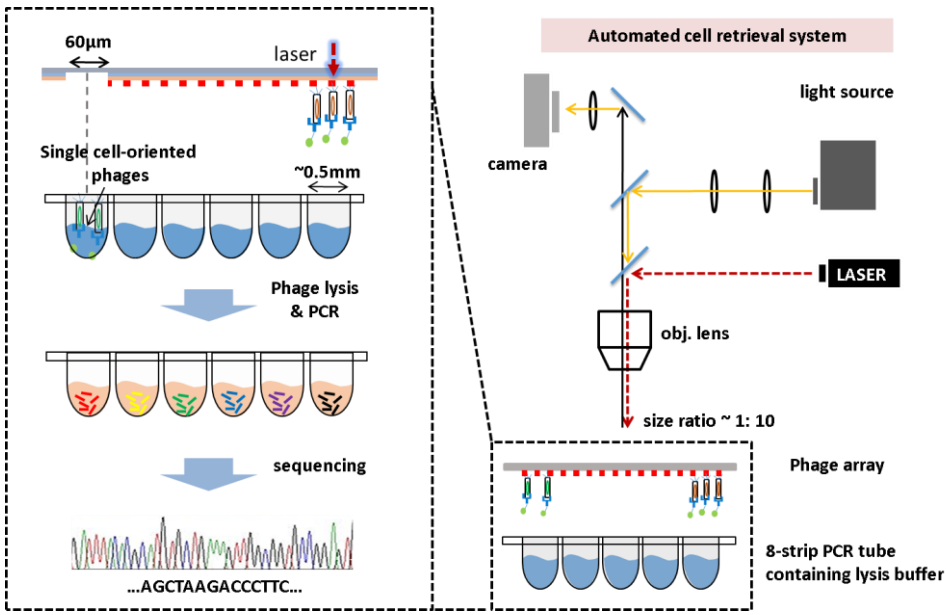

Figure 2.18 Schematic of automated laser-driven sample retrieval system. Targeted samples were isolated by infrared laser system to 8-strip PCR tube conining lysis buffer, and then isolated phages were lysed and amplified by PCR. To confirm sequences of retreieved phages, obataind clones were sequenced by the Sanger method.

Before the sequencing by the Sanger method, the retrieval efficiency was validated by using gel electrophoresis. The results of gel electrophoresis were shown in figure 2.19(a). All samples successfully produced an amplicon with the target length, 1kbps. There was also no damage in the antibody sequence, as shown in figure 2.19(b). Only CDRs were shown high-variability.

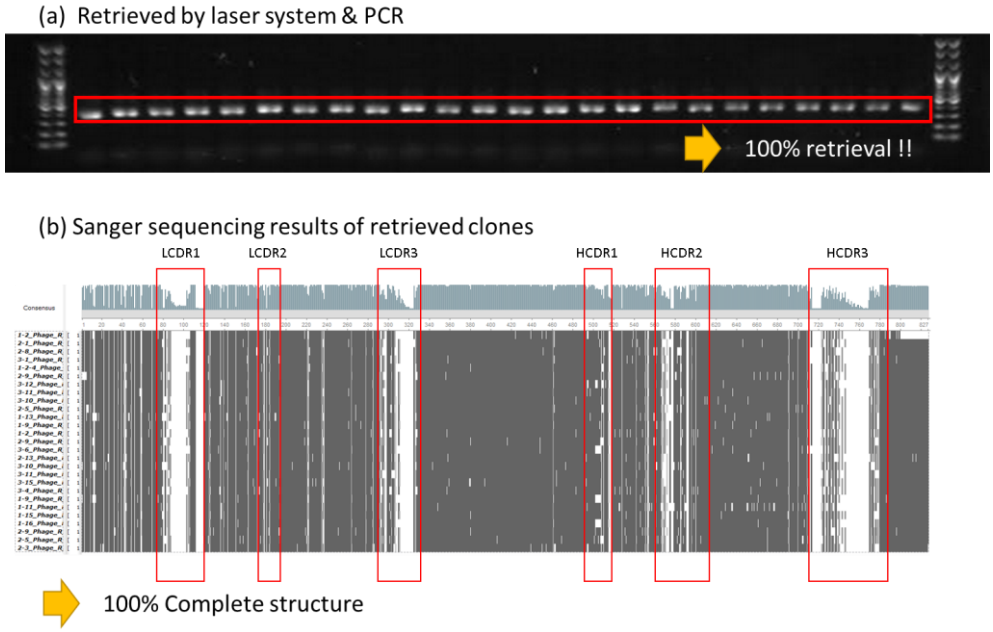

Figure 2.19 (a) The results of gel electrophoresis. Every selected clones were successfully isolated and amplified. (b) The results of the Sanger sequencing. Only CDRs had variability that suggsted there was no damage in the antibody sequence during laser isolation.

2.4. Analysis of genotype and phenotype of retrieved samples

2.4.1. The high-throughput analysis of retrieved clones

For high-throughput analysis of the collected samples, multiple samples were pooled into a single tube before the phage lysis and converted into a phagemid vector form after the amplification. After transfection of converted phagemid, individualization of the pooled sample, and high-throughput barcoded colony sequencing were performed by using TrueRepertoire™ (TR™, Celemics) [33]. The sequencing result was analyzed by using a Python script written for the identification of scFv clones.

In order to confirm that the identified clones had a sufficient binding affinity, phages were rescued from the individualized colony samples and subjected to phage ELISA [40]. Briefly, phages were rescued using helper phage, and microtiter plates were coated with antigen. The plates were sequentially incubated with scFv-displaying phages and reporter-conjugated antibody. Absorbance was measured with a microplate reader (Figure 2.20).

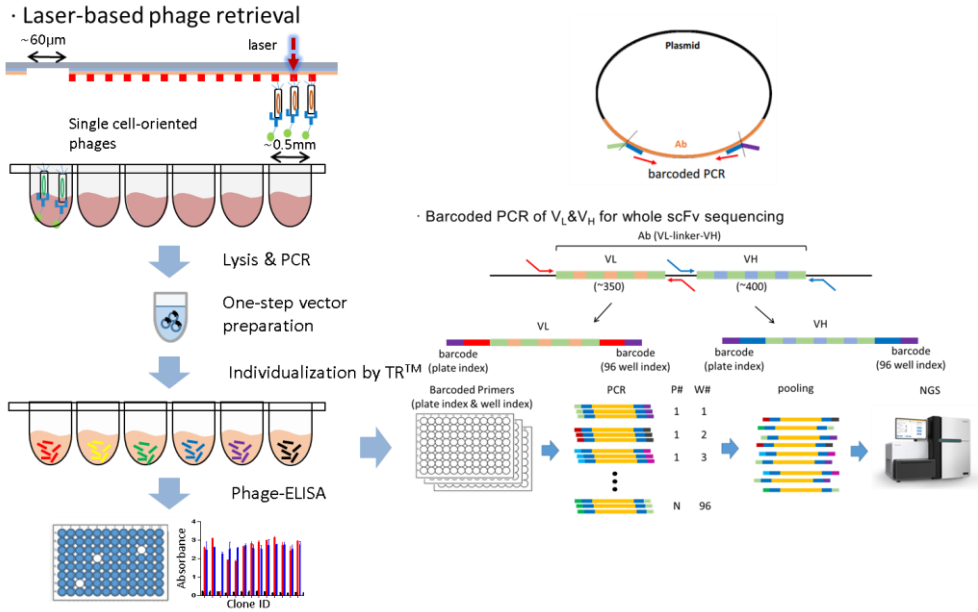

Figure 2.20 Schametic of high-throughput analysis of collected phages. The isolated phages collected into one tube for one-step vector transformation. After the transfection of prepared phagemid, cells were individualized by TR™. Individulized colonies were sequences by barcoded PCR and NGS and measured the affinity agatinst target antigen using phage-ELISA.

2.5. Validation of the whole process

2.5.1. Validation test in various positive rate libraries

For validation experiments, three anti-human HGF scFvs and an anti-cotinine scFv (P1, P2, P3, and N in this dissertation) were provided by Prof. Junho Chung(Seoul National University College of Medicine) after conventional phage display of a naive library against hHGF and cotinine [41]. Each scFv gene was inserted into a phagemid vector and phage encoding P1, P2, P3 or N were mixed at the desired dilutions for use as an alternative for the phage library to be screened against human HGF. N phage used as a negative clone against hHGF.

The mixture of P1, P2, P3 positive clones(1:1:1 ratio) was mixed at a 1:0, 1:10, 1:100 ratio with the negative clone. The final mixed phage solution infected cells and loaded into the microwell array chip with helper phage. After overnight incubation to allow phage production and capture on the antigen-coated surface, the microwell array was disassembled and labeled the captured phages. As a result, approximately 99%, 10%, 0.5% of the clones were positive, coincident with 100%, 10%, 11% of the input clones were positive clones (Figure 2.21). Figure 2.21(b) shows the number of high-intensity clones was shifted to no intensity clones following a decreased positive rate of input clones.

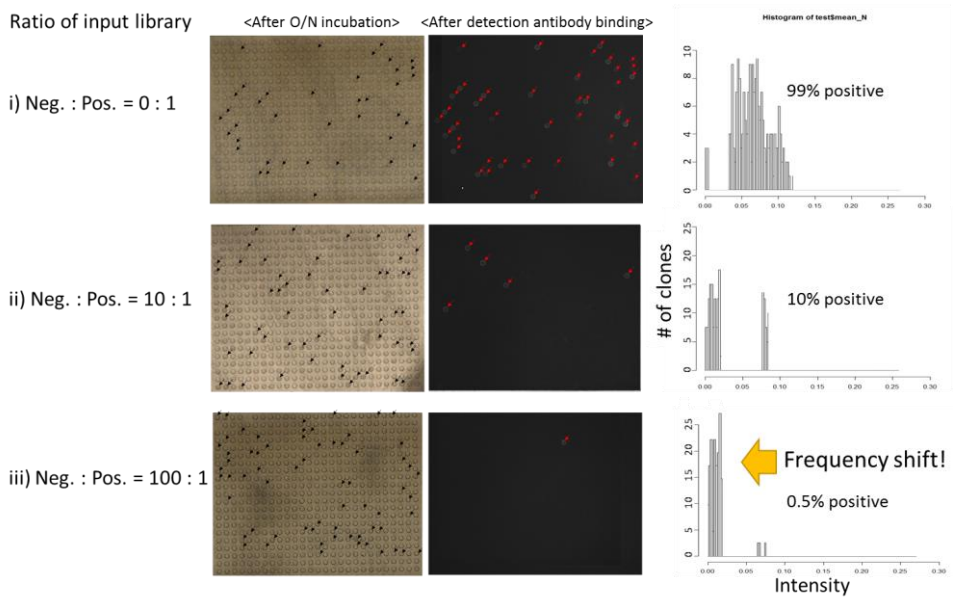

Figure 2.21 The positive clones was mixed at a 1:0, 1:10, 1:100 ratio with the negative clone. (a) As the positive rate decrease, the number of wells with fluorescence signal was also decreased. (black arrow: wells occupied by cells, red arrow: fluorescence signal of wells) (b) The number of high-intensity clones were shifted to low-intensity.

According to the results of the Sanger sequencing, the selected clones were that three positive clones with approximately 3:1:2 ratio(1:1:1 ratio in the input mix), no negative clone. The sequences of P1 and P2 clones were almost the same, but slightly different in LCDR2 and LCDR3, and much different from P3 in every CDRs (Figure 2.22). Since the ratio of three positive clones in results of the Sanger sequencing closely matched the input ratio, this data confirms the Million-ELISA that sensitive enough to distinguish specific binders from non-binders. Interestingly, the overall

fluorescence of the P2 phages was lower than the fluorescence of P1, P3, possibly reflecting differences in antibody affinities[29].

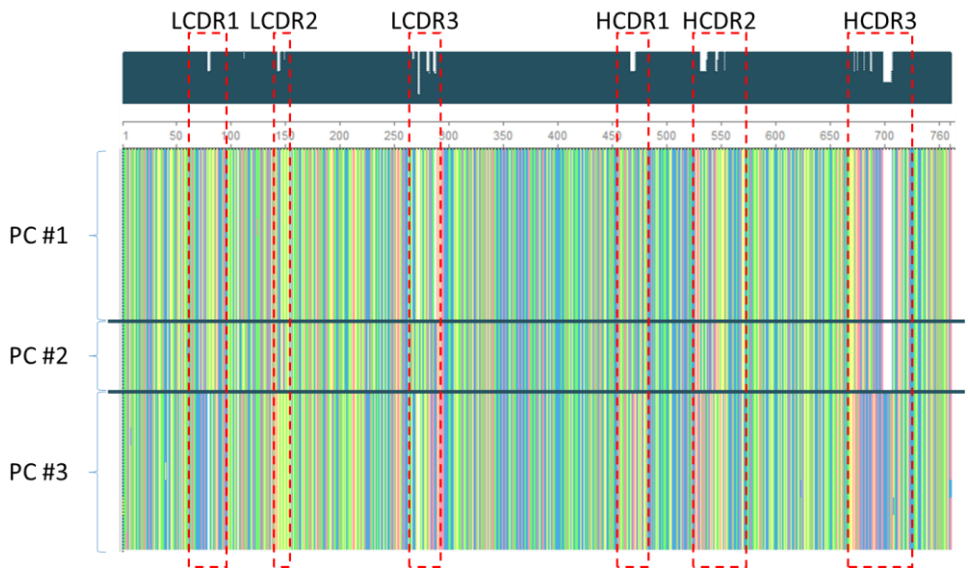

Figure 2.22 The alignment of sequences analyzed by the Sanger sequencing. The selected clones were three positive clones with approximately 3:1:2 ratio (1:1:1 ratio in the input mix), no negative clone. Since the output ratio of three positive clones closely matched the input ratio, this result suggests that the proposed platform is sensitive enough to discriminate specific binders from nonbinders.

2.5.2. Validation test in each panning round library - from 1st to 4th

For validation in the actual antibody library, each round of output library obtained during four panning rounds against Prostate-specific antigen (PSA). Application results showed that the four and seven positive clones per chip were detected in first and second round panning rounds. In the third round panning library, there were 995 positive clones per chip, a 140-fold increase from second round panning. The detected positive clones from the fourth round panning library were 15960, a 15-fold increase (Figure 2.23). As expected, the enrichment of the library by multiple rounds of panning increased the proportion of positive clones. The positive rate of the first panning and second panning, however, were analogous, suggesting that the result of first round panning included false positives. Of the positive clones detected in the fourth round panning library, 137 clones were isolated and sequenced for comparing with the result of conventional phage display. The 123 of 137 clones were five unique sequences analyzed by the Sanger sequencing and were identified as positive clones in the conventional phage display method. The most frequent sequence among the five unique sequences accounted for 75% of the total population, indicating that certain clones were enriched during four rounds of panning. The other 14 clones were analyzed as negative clones, and 90% of the retrieved clones were identified as a positive clone (Table 2.1).

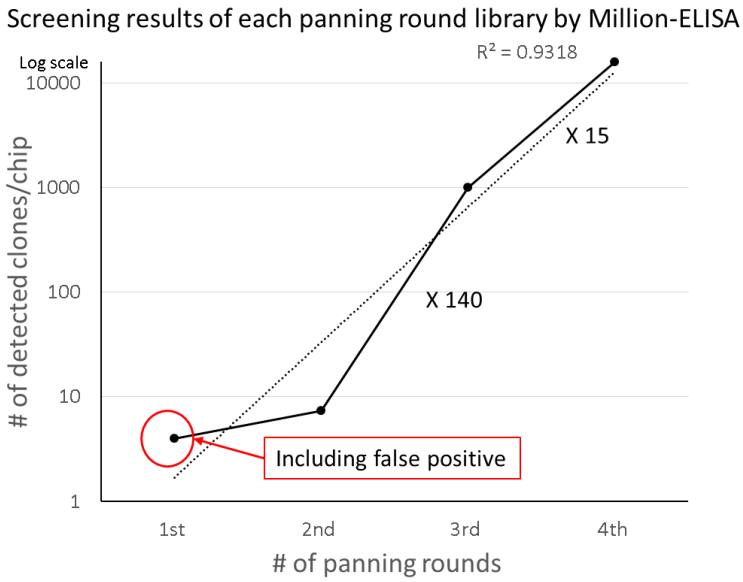

Figure 2.23 The number of detected clones per chip in each panning round library. The first and second round panning rounds showed almost same number of positive clones. In the third round panning library, a 140-fold increase from second round panning. The detected positive clones from the fourth round panning library were increased to a 15-fold.

Sequencing result of retrieved clones from 4th panning round

*positive #1~5 were also detected by Bio-panning method

	Positive #1	Positive #2	Positive #3	Positive #4	Positive #5	Negative clones	SUM
total	93	21	1	6	2	14	137

Table 2.1 The results of analyzed the fourth round panning library by proposed platform. 123 clones out of isolated 137 clones were five unique sequences and identified as positive clones in the conventional phage display method.

Chapter 3.

Application: Screening of Deimmunization library

In this chapter, I will describe an application of the proposed platform. The microwell array chip and automated laser retrieval system developed for high-throughput phage display make it easy to reduce the number of panning round that is essential to minimize the loss of binders. Different from other screening technology which has complicated sample isolation approaches and is prone to cross-contamination, the use of single-cell level approach in combination with an elaborate sample retrieval method enables high-throughput sample retrieval at minimal amplification bias as well as sample cross-contamination.

I applied this platform for the screening of a deimmunization library of targeted CD28 antigen. Using the developed phage display platform, screening of synthetic deimmunization library is demonstrated, obtaining novel antibody clones that were not detectable in the conventional biopanning method. At the beginning of the chapter, I will describe the clinical and biological meaning of the deimmunization

library in more detail. Then, the screening result of the proposed platform will be presented.

3.1. Therapeutic Benefit of the deimmunization

Immunogenicity of therapeutic antibodies can drive an anti-drug immune response that compromises efficacy and even undermines safety [42]. A major reason for immunogenicity is the presence of human T-cell epitopes within the antibody sequence which can activate helper T-cells resulting in the supported production of antibodies and neutralization of the therapeutic effect [43].

Removal of T-cell epitopes has been termed ‘‘deimmunization’’ [44]. Chimeric and humanization technologies seek to maximize the content of amino acids derived from other human antibody sequences, which could not eliminate T-cell epitopes. Therefore, a further improvement of these technologies is to identify and eliminate T-cell epitopes from the variable regions of antibodies [45]. To eliminate T-cell epitopes in antibody, mutations to remove T-cell epitopes can generally be introduced without significantly reducing the binding affinity of the antibody. The antibody library in which the original antibody sequence is mutated to remove T-cell epitopes is called the "deimmunization library" (Figure 3.1).

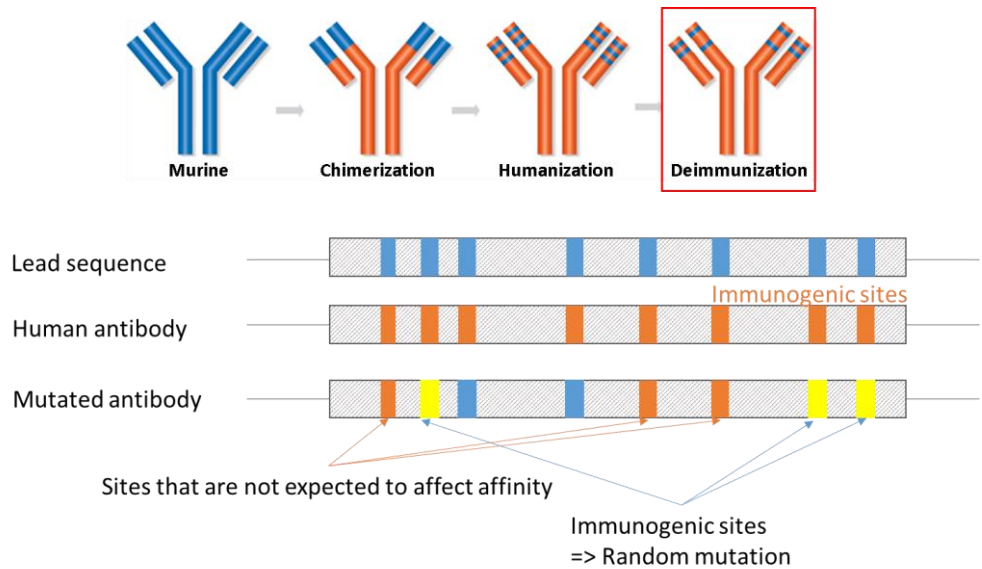

Figure 3.1 How to designe “deimmunization” library. To eliminate T-cell epitopes in antibody, mutations to remove T-cell epitopes can generally be used.

3.2. Screening of Deimmunization library against CD28 antigen using the proposed high-throughput phage display method

3.2.1. Experimental procedure

Microwell array chip was prepared by assembling a microwell array and a sample-capturing substrate. The microwell array was fabricated using soft-lithography in which polydimethylsiloxane (PDMS, SYLGARD 184, Dow Corning) was cast onto a silicon mold having SU-8 photoresist pattern (SU-8 2015, Microchem) and cured for 1 hour at 95 ℃. The cured 3mm-thick PDMS block having a two-dimensional array of microwells (d 60μm, h 40μm) was obtained by

peeling off from the mold. The sample-capturing substrate was prepared by forming a target-capturing layer on top of an Indium tin oxide (ITO) coated glass slide (ITO thickness 100nm, Fine Chemicals Industry, Seoul, Korea). For the target-capturing layer formation, a mixture of 3.4mL of (7.0-8.0% vinylmethylsiloxane) - dimethylsiloxane copolymer (VDT-731), 18μl of platium-divinyltetramethyldisiloxane (SIP6831.2LC), 100μl of 1,3,5,7-tetravinyl-1,3,5,7-tetramethylcyclotetrasiloxane (SIT7900.0) and 1mL of (25-35% methylhydrosiloxane) - dimethylsioloxane copolymer (HMS-301, all from Gelest) was spin-coated and thermally cured, yielding a polymeric layer with a thickness of 3um. The microwell array and the sample-capturing substrate were directed to each other and fixed by using a custom-made chip holder consisting of aluminum plate and acryl sheet. The chip holder was designed to fit into conventional microplate reader format and allow optical imaging through a transparent window while maintaining reliable compartmentalization of individual microreaction chambers by tightening screws.

For deimmunization screening, a pre-discovered anti-CD28 scFv clone was selected as a randomization template in which five amino acid sites were mutated (RMN/YMY/NNK/MTN/RYN), yielding a synthetic library with a size of 5.21x10^5 (Table 3.1). The microwell array and the sample-capturing substrate were treated with an oxygen plasma (CUTE, Femto Science) for 2 minutes. The plasma-treated pair was then immersed in an antigen solution (5μg/mL in 0.1M sodium bicarbonate buffer, pH 8.6) for 90 minutes at 37℃, followed by blocking with 3%

BSA (in PBS) for 1 hour at room temperature. Escherichia coli (E.coli) cells (ER2738, New England Biolabs) were grown in 300μL of Super Broth(SB) medium at 250rpm/37℃. Once the OD at 600nm reached ~ 0.7, 30μL of prepared phages(6x10^7 cfu/ml) was added. E.coli cells were held at room temperature for 15 minutes without shaking to allow phage infection. A 1336μL of SB medium containing carbenicillin was added(16μg/mL). E.coli cells were incubated for 1 hour at 250rpm/37℃. After 24μL of carbenicillin was added(40μg/mL), E.coli cells were incubated at 250rpm/37℃ for an additional hour. A suspension of E.coli(OD 0.3~0.5) cells was diluted to 2 x 10^7 in the helper phage solution containing M13K07 helper phage(10^11 CFU/mL) and carbenicillin(50μg/mL). The diluted E.coli solution was immediately loaded into the microwell array.

Right after loading of E.coli solution, the microwell array was mounted on the chip holder with the target-capturing substrate in order to isolate individual microwells. The chip-loaded holder was incubated overnight at 37℃ to allow cell growth and phage production within microwells. The microwell array chip was disassembled back to the microwell array and the target-capturing substrate, each of which was washed with PBS/Tween20 (0.05%, PBST). The microwell array was immersed in 3% BSA (in PBS) for 1 hour at room temperature, followed by incubation with FITC-conjugated anti-M13 antibody (61R-M101AFT, Fitzgerald) for the purpose of fluorescence labeling of surface-bound phage molecules. The labeled microwell array was washed with PBST, assembled with a non-treated glass

slide, and mounted to the chip holder for subsequent imaging. The target-capturing substrate was also treated with the same blocking and labeling conditions in validation experiments.

Brightfield and fluorescence images of the microwell array chip were acquired by using an automated fluorescence microscope (Ti-E, Nikon) equipped with a high-sensitivity charge-coupled device camera (C11440, Hamamatsu). For fluorescence imaging, a 470nm excitation condition (SpectraX 6-NII-SA, lumencor) was used in combination with a FITC filter unit (excitation peak ~ 490nm, emission peak ~ 525nm). In all imaging conditions, a whole microwell area within the microwell array chip was scanned through a 4x objective lens, generating a series of microscope. The image acquisition process was performed before and after the disassembly of the microwell array chip, respectively.

The acquired individual images were stitched into a large reconstructed image showing the whole microwell area of a single microwell array chip. In order to provide the positions of target samples to be retrieved from the chip, a Python script for image analysis was developed and utilized. To be more specific, coordinates of individual microwells and the corresponding fluorescence intensities were firstly extracted from the stitched images. By comparing the coordinates of the microwells and on-chip alignment markers obtained before and after the chip disassembly, target sample positions on the sample-capturing substrate were then determined. The obtained positions of the target samples were finally converted into the form of the displacements needed for the operation of a laser-based sample retrieval system.

The sample retrieval system developed by our group was utilized under the control of a Python script written for this work. Briefly, two independent 3-axis mechanical stages and an infrared pulse laser (MiniliteTM Series ML II; Continuum) were operated in a synchronized manner in order to selectively separate phage of interest from the surface of the target-capturing substrate. The retrieved phage molecules were collected in an 8-strip PCR tube filled with 7μl of phage lysis buffer (1% Triton X-100, 500 mM Guanidine-HCl, 10mM MOPS, pH 6.5), followed by 20 minutes incubation at 80℃ for lysis of phage coat protein. Phage viral DNA covering the scFv region was then amplified using Jumpstart DNA polymerase (D9307, Sigma Aldrich) and sequenced by the Sanger method. For high-throughput analysis of the collected samples, multiple samples were pooled into a single tube before the phage lysis and converted into a plasmid vector form after the amplification. High-throughput barcoded colony sequencing and individualization of the pooled sample were performed by using TrueRepertoire™ (Celemics). The sequencing result was analyzed by using a Python script written for the identification of scFv clones and mutations. In order to confirm that the identified clones had a sufficient binding affinity, phages were rescued from the individualized colony samples and subjected to phage ELISA.

	RMN	**YWY**	**NNK**	**MTN**	**RYN**
Charged (+)	Lys(K)	His(H)	Arg(R) His(H) Lys(K)		
Charged (-)	Asp(D) Glu(E)		Asp(D) Glu(E)		
Uncharged	Asn(N) Thr(T)		Ser(S) Thr(T) Asn(N) Gln(Q)		Thr(T)
Special cases			Cys(C) Gly(G) Pro(P)		
Hydrophobic	Ala(A)	Leu(L) Phe(F) Tyr(Y)	Ala(A) Val(V) Ile(I) Leu(L) Met(M) Phe(F) Tyr(Y) Trp(W)	Ile(I) Leu(L) Met(M)	Ala(A) Val(V) Ile(I) Met(M)
			Stop(*)		

Table 3.1 Amino acids available at each mutation site. A pre-discovered anti-CD28 scFv clone was selected as a randomization template in which five amino acid sites were mutated (RMN/YMY/NNK/MTN/RYN).

3.2.2. The results of Screening of Deimmunization library using the proposed high-throughput phage display

To verify that the entire process was working as intended before high-throughput analysis, the deimmunization library applied to two microarray chips, and detected clones were isolated and sequenced by the Sanger method. The results showed that the library had a positive rate of approximately 0.5~0.6% (Figure 3.2(a)), and isolated 24 clones from each chip. 38 out of 48 clones were successfully isolated (Figure 3.2(b)), and 32 clones were sequenced by the Sanger method.

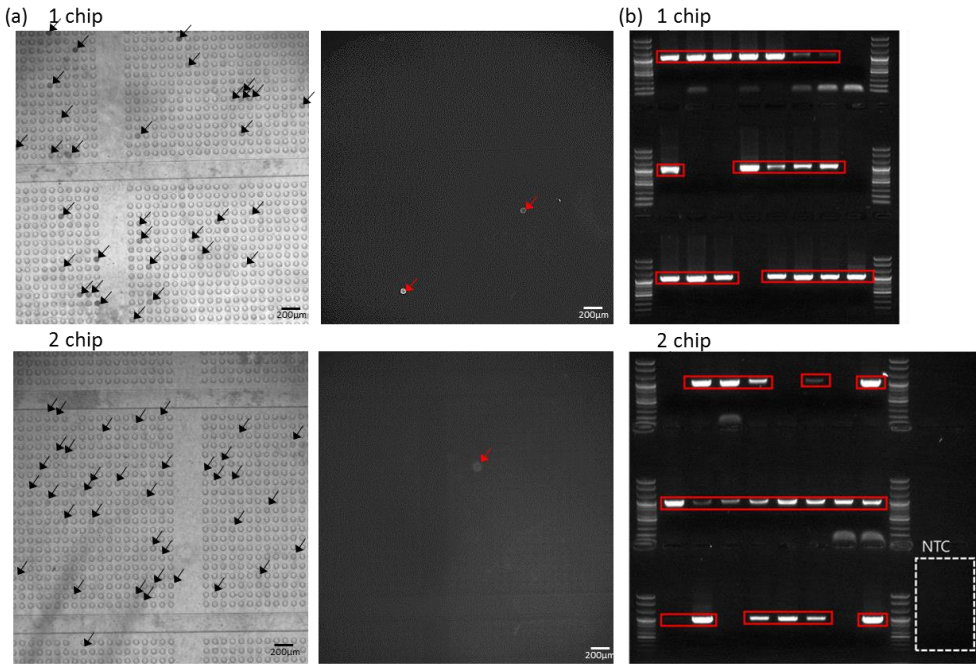

Figure 3.2 The results of two chip applied for deimminization library. (a) Images of assembled microwell array chips, after overnight incubation(left). Fluorescence images of labeled microwell array(right). Black arrow: cell grown wells, red arrow:

fluorescen signal of microwells. (b) In the two chips, 24 clones isolated from each chip and 38 out of 48 clones were successfully isolated

In alignment of sequences obtained as a result of the Sanger method, the sequences were different only at mutated five sites (Figure 3.3). The proposed platform was perceived to be working as intended, and an additional seven chips(70,000 assays) were used to analyze 14% of the whole library. A total of 318 clones were detected and isolated. The retrieved clones were pooled into a single tube and converted into a vector form. Individualization of the pooled sample and high-throughput barcoded colony sequencing were performed by using TrueRepertoire^{TM} (Celemics). Phages were rescued from the individualized colony samples and subjected to phage ELISA for confirming the identified clones had a binding affinity.

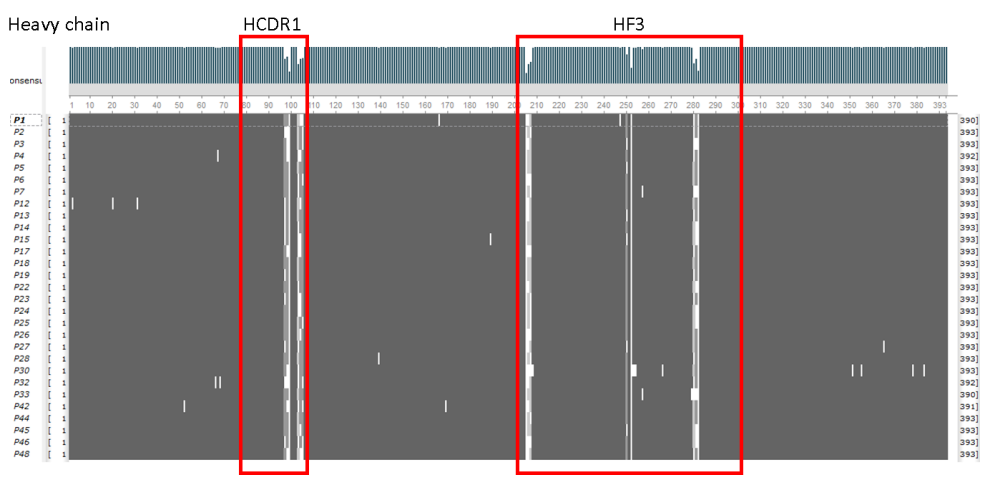

Figure 3.3 The alignment of isolated clones from deimmunization library. Only

mutated five sites were shown various.

The sequencing result was analyzed by using a Python script written for identification of scFv clones and mutations as following: (i) Light and heavy chain sequences were extracted from the obtained reads by aligning to the vector and scFv linker sequence. (ii) The sequences having unintended mutations were excluded. (iii) The sequences found to have amino acid mismatches (except mutation sites) compared to the template sequence were filtered out (Table 3.2).

The result of the sequencing was analyzed based on the number of counts and unique clones. As a result of sequencing, 203 out of retrieved 318 clones were analyzed, and among 112 clones were positive clones. After excluding clones with unintended mutations, the sequences that have more than six mismatches with the template sequence were also excluded. A total of 199 clones were filtered, of which 112 clones were identified as positive clones. The positive rate of the number of clones was 56.2%, but the positive rate was 93.4% based on the counts. This difference was mitigated to 69.4% and 96.1% if the filtering condition was harsher to perfect match the templates. There was still, however, a difference in the positive rates.

	# of counts	Positive rate	# of clones	Positive rate
# of isolated clones			318	
TR data(AA seq)	2984		203	
Template mismatch(≤5)	2977		199	
Positive	2780	93.4%	112	56.2%
Template match	2797		62	
Positive	2689	96.1%	43	69.4%

Table 3.2 The results of NGS in TR™ analysis. As a result of sequencing, 203 out of retrieved 318 clones were analyzed, and among 112 clones were positive clones.

The reason was that in the process of pooling the retrieved phages into one tube for high-throughput analysis, the repetitively retrieved phages were not identified as an individual clone and analyzed as one clone. The counts of the most frequent clones and second most frequent clones were 1883 and 584, respectively, accounting for about 2/3 of the total number of 2984 counts, suggesting that there were repetitively retrieved clones. In the magnified graph, the red bars were positive clones, and most of the clones that had high counts were the positive clones (Figure 3.4). In other words, since repetitively retrieved clones were positive clones, the positive rate based on the counts was higher than it based on the number of clones. To verify more clearly, the clones were divided by the counts. When the counts were more than 3, the positive rate was 80%, and when the counts were lower than 2, only half of the clones were positive, verifying that the positive clones were repetitively isolated (Table 3.3).

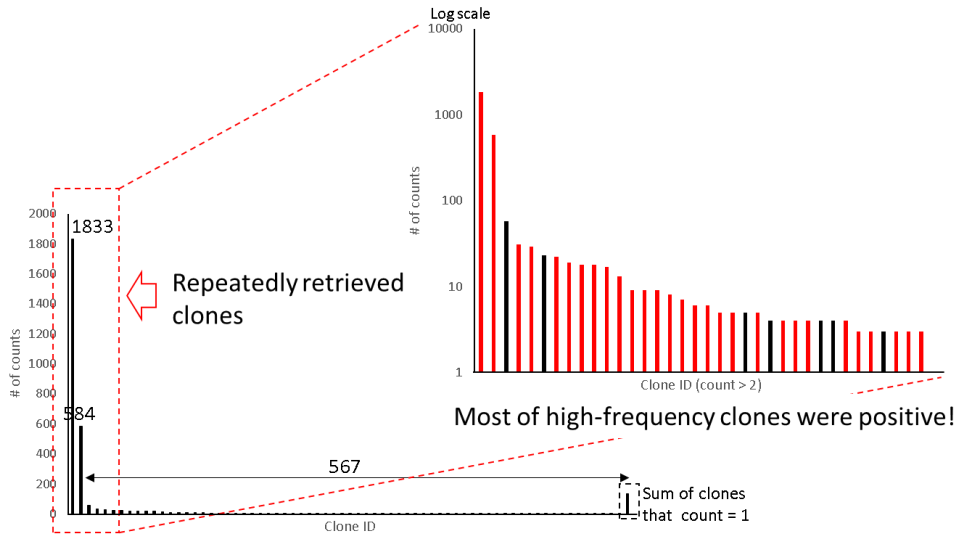

Figure 3.4 The frequency of analyzed clones by NGS. The most frequent clones and second most frequent clones were 1883 and 584, respectively, suggesting that there were repetitively retrieved clones. In the magnified graph, the red bars were positive clones, and black bars were negative clones. The most of the clones that had high counts were the positive.

	Positive	Negative	Total	Positive rate
Count > 2	29	7	36	80.6
Count ≤ 2	83	80	163	50.9
Total	112	87	199	56.3

Table 3.3 The results of NGS in TR™ analysis based on counts. When the counts were more than 3, the positive rate was 80%, and when the counts were lower than

2, only half of the clones were positive.

Distribution of amino acid sequences was obtained from the identified scFv clones binding to the target antigen. Since the RMN/YWY/NNK/MTN/RYN mutations were given at each of the five sites, the amino acid sequences that could be present in each site were different. Two mutation sites were in the HCDR1, and three mutation sites were in the HF3 (Table 3.4).

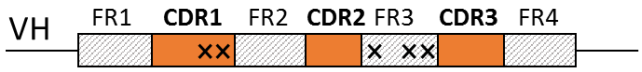

	RMN	YWY	NNK	MTN	RYN
Charged (+)	Lys(K)	His(H)	Arg(R) His(H) Lys(K)		
Charged (-)	Asp(D) Glu(E)		Asp(D) Glu(E)		
Uncharged	Asn(N) Thr(T)		Ser(S) Thr(T) Asn(N) Gln(Q)		Thr(T)
Special cases			Cys(C) Gly(G) Pro(P)		
Hydrophobic	Ala(A)	Leu(L) Phe(F) Tyr(Y)	Ala(A) Val(V) Ile(I) Leu(L) Met(M) Phe(F) Tyr(Y) Trp(W)	Ile(I) Leu(L) Met(M)	Ala(A) Val(V) Ile(I) Met(M)
			Stop(*)		

Table 3.4 The possible amino acids in five mutation sites. Red letters were the most

frequenct amino acids in the result of screening by the proposed platform.

There were the mutated amino acid sequences in a similar ratio prior to screening but after screening by propose platform, amino acid sequences tended to be biassed against specific sequences (Figure 3.5). In the first site, Thr, Asn, Asp accounted for more than 80% of the total, and in the second site, Phe and Tyr accounted for more than 70%. In the third site, the most diverse amino acids were shown because of the NNK mutation, with Ala biased to occupy almost half the population. In the fourth site, two of three amino acids accounted for the vast majority. In the fifth site, the degree of bias was not severe compared to other sites, but the population of the most frequent amino acid and the second most frequent amino acid was about 2 times different. This biased pattern will be an important reference in the design of the library in the future.

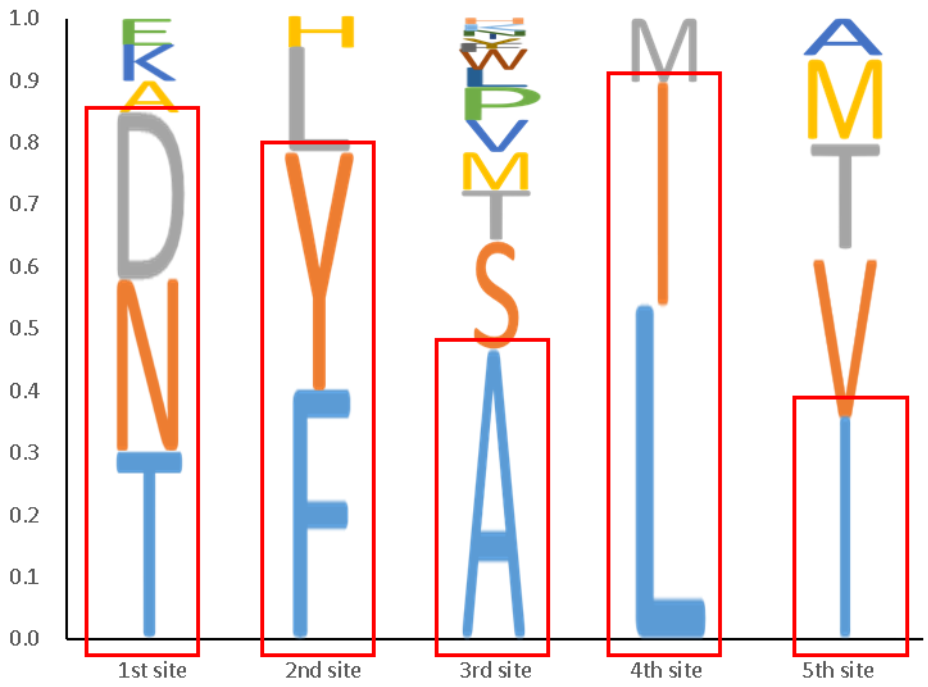

Figure 3.5 The distribution of amino acid in the mutated sites. In the first site, T, N, D accounted for more than 80% of the total, and in the second site, F and Y accounted for more than 70%. In the third site, A occupied almost half the population. In the fourth site, L and I accounted for the vast majority. In the fifth site, I was the most frequent amino acid.

The results of analysis using the proposed platform and conventional phage display were compared. The same deimmunization library was analyzed by both methods. The proposed platform analyzed 14% of the whole library, but the conventional phage display analyzed only 0.01% (Figure 3.6(a)). The screen size of the proposed platform was 200 times larger than the conventional method. The

proposed platform revealed a total of 112 positive clones, novel clones six times more than the conventional method that detected only 19 positive clones. Only one clone was detected in both methods, so this platform uncovered 111 novel antibodies (Figure 3.6(b)).

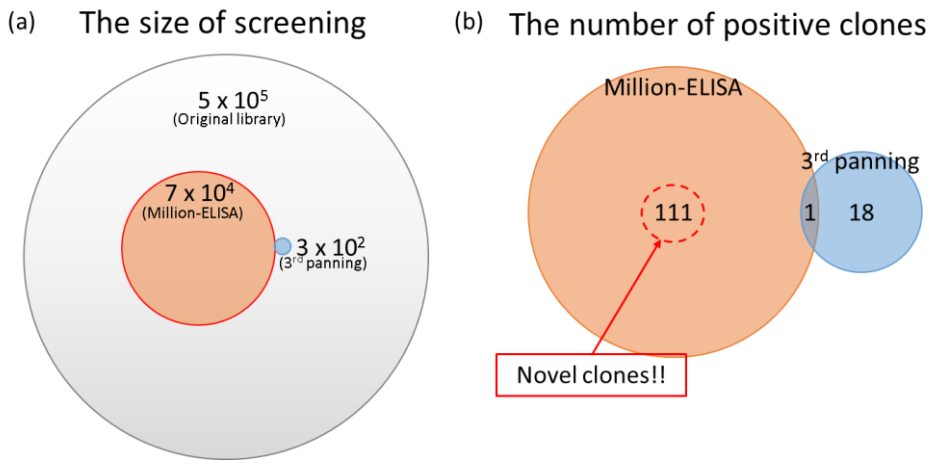

Figure 3.6 The proposed platform vs conventional phage display. (a) The proposed platform analyzed 14% of the whole library, but the biopanning method analyzed only 0.01% through 3 round panning. (b) The proposed platform dicovered 112 positive clones, and the conventional method detected only 19 positive clones. Only one clone was detected in both methods.

Chapter 4.

Conclusion and Discussion

Phage display is the most widely used technology for screening potential candidates of antibody libraries. Phages can display the desired peptides as a component of their surface proteins. In the phage display, scFv was expressed on the surface of phages for antibody selection. Phage display, however, has some technical limits, such as time-consuming, laborious work, the limited screen size, the loss of binders. Due to the limited screen size, multiple rounds of panning were required for the enrichment of positive clones. The loss of binders is getting worse during the 3~5 round panning.

In this dissertation, I developed the high-throughput phage display method using the microwell array chip and the automated laser-driven retrieval system. The microwell array chip improved the throughput of the assay to 10,000 clones at one chip. I developed a hybrid holder structure that combined the acryl sheet and aluminum plate to maintain the assembled microwell array chip. Designed holder reduced cross-contamination between microwells during incubation. I also

developed the microwell array chip that had independent substrates for detection and phage retrieval for advantageous in preventing cross-contamination. The pattern of well structures allowed easier detection than a flat surface. I developed systems separated by detection and retrieval, which can support a clear in-well image and prevention of cross-contamination. I developed the additional layer that deposited on the sacrificial layer to minimize the loss and damage of retrieved phages. The sacrificial layer(ITO) absorbed the energy of the laser and vaporized. Developed h-PDMS layer prevented scattering of captured phages. Therefore, the automated laser-driven system and optimized target-capture layer maximized the throughput and minimized the contamination and damage of the clone.

As an application, I demonstrated the ability to identify novel antibodies in a scalable de-immunization library against CD28. For deimmunization screening, a pre-discovered anti-CD28 scFv clone was selected as a randomization template in which five amino acid sites were mutated (RMN/YMY/NNK/MTN/RYN), yielding a synthetic library with a size of 5.21x10^5. In this dissertation, I screened 14% of the whole library and detected 112 positive clones without panning. In the conventional phage display, 19 positive clones were obtained through three rounds of panning. Only one clone was detected in both methods. The proposed platform uncovered 111 novel antibodies that could not be detected by the conventional method. In conclusion, this method enables high-throughput screening to reduce the number of panning rounds, which increases the possibility of discovering clones previously undetectable. For the future work, this platform will be used for

application where the affinity maturation library and naive library in addition to the deimmunization library. This platform could be used to analyze the antibody library as well as cells that secrete antibodies or specific molecules, such as a cytokine, interleukin in the future.

.

Bibliography

[1] EvaluatePharma, “World Preview 2018, Outlook to 2024,” 2018.

[2] H. L. L. Dawn M Ecker, Susan Dana Jones, “The therapeutic monoclonal antibody market,” *MAbs*, vol. 7, no. January/February 2015, pp. 9–14, 2015.

[3] PharmaIntelligions, “Top 10 Best-Selling Drugs of 2018 Fund US and EU Pharma R & D,” 2018.

[4] I. G. Research, “Monoclonal Antibody Therapeutics Market: Global Industry Analysis, Trends, Market Size, and Forecasts up to 2025,” 2019.

[5] Inovation.orf, “Drug discovery and development,” 2007.

[6] J. Zurdo, “Developability assessment as an early de-risking tool for biopharmaceutical development,” *Pharm. Bioprocess.*, vol. 1, no. 1, pp. 29–50, 2013.

[7] S. M. Paul *et al.*, “How to improve RD productivity: The pharmaceutical industry’s grand challenge,” *Nat. Rev. Drug Discov.*, vol. 9, no. 3, pp. 203–214, 2010.

[8] H. Xue, J. Li, H. Xie, and Y. Wang, “Review of drug repositioning approaches and resources,” *Int. J. Biol. Sci.*, vol. 14, no. 10, pp. 1232–1244, 2018.

[9] R. A. Brodsky, “How I treat paroxysmal nocturnal hemoglobinuria,” *Blood*, vol. 113, no. 26, pp. 6522–6527, 2009.

[10] T. university of Arizona, “The biology project-Immunology,” *Online Information Review*, 2000. [Online]. Available: http://www.biology.arizona.edu/immunology/tutorials/antibody/structure.html.

[11] L. Ledsgaard, M. Kilstrup, A. Karatt-Vellatt, J. McCafferty, and A. H. Laustsen, “Basics of antibody phage display technology,” *Toxins (Basel).*, vol. 10, no. 6, 2018.

[12] S. Sharma *et al.*, “Characterization of a putative ovarian oncogene, elongation factor 1α isolated by panninga synthetic phage display

single-chain variable fragment library with cultured human ovarian cancer cells," *Clin. Cancer Res.*, vol. 13, no. 19, pp. 5889-5896, 2007.
[13] S. Carmen and L. Jermutus, "Concepts in antibody phage display," *Briefings Funct. Genomics Proteomics*, vol. 1, no. 2, pp. 189-203, 2002.
[14] J. Bazan, I. Całkosiñski, and A. Gamian, "Phage displaya powerful technique for immunotherapy: 1. Introduction and potential of therapeutic applications," *Hum. Vaccines Immunother.*, vol. 8, no. 12, pp. 1817-1828, 2012.
[15] P. A. C. 'T Hoen *et al.*, "Phage display screening without repetitious selection rounds," *Anal. Biochem.*, vol. 421, no. 2, pp. 622-631, 2012.
[16] C. M. Y. Lee, N. Iorno, F. Sierro, and D. Christ, "Selection of human antibody fragments by phage display.," *Nat. Protoc.*, vol. 2, no. 11, pp. 3001-3008, 2007.
[17] R. Peltomaa, E. Benito-Peña, R. Barderas, and M. C. Moreno-Bondi, "Phage display in the quest for new selective recognition elements for biosensors," *ACS Omega*, vol. 4, no. 7, pp. 11569-11580, 2019.
[18] P. Mondon, O. Dubreuil, K. Bouayadi, and H. Kharrat, "Human antibody libraries: A race to engineer and explore a larger diversity," *Front. Biosci.*, vol. 13, pp. 1117-1129, 2008.
[19] R. Derda, S. K. Y. Tang, S. C. Li, S. Ng, W. Matochko, and M. R. Jafari, "Diversity of phage-displayed libraries of peptides during panning and amplification," *Molecules*, vol. 16, no. 2, pp. 1776-1803, 2011.
[20] W. L. Matochko, S. Cory Li, S. K. Y. Tang, and R. Derda, "Prospective identification of parasitic sequences in phage display screens," *Nucleic Acids Res.*, vol. 42, no. 3, pp. 1784-1798, 2014.
[21] G. Walter, Z. Konthur, and H. Lehrach, "High-throughput Screening of Surface Displayed Gene Products," *Comb. Chem. High Throughput Screen.*, vol. 4, no. 2, pp. 193-205, 2012.
[22] S. J. McConnell, T. Dinh, M. H. Le, and D. G. Spinella, "Biopanning phage display libraries using magnetic beads vs. polystyrene plates," *Biotechniques*, vol. 26, no. 2, pp. 208-214, 1999.
[23] C. Rhyner, Z. Konthur, K. Blaser, and R. Crameri, "High-throughput isolation of recombinant antibodies against recombinant allergens," *Biotechniques*, vol. 35, no. 4, pp. 672-674, 2003.
[24] L. Turunen, K. Takkinen, H. Söderlund, and T. Pulli, "Automated panning and screening procedure on microplates for antibody generation from phage display libraries," *J. Biomol. Screen.*, vol. 14, no. 3, pp. 282-293, 2009.
[25] B. Krebs *et al.*, "High-throughput generation and engineering of recombinant human antibodies," *J. Immunol. Methods*, vol. 254, no. 1-

2, pp. 67–84, 2001.
[26] D. J. Schofield *et al.*, “Application of phage display to high throughput antibody generation and characterization,” *Genome Biol.*, vol. 8, no. 11, 2007.
[27] M. M. Kiss *et al.*, “Phage ESCape: An emulsion-based approach for the selection of recombinant phage display antibodies,” *J. Immunol. Methods*, vol. 367, no. 1–2, pp. 17–26, 2011.
[28] V. Fitzgerald *et al.*, “Exploiting highly ordered subnanoliter volume microcapillaries as microtools for the analysis of antibody producing cells,” *Anal. Chem.*, vol. 87, no. 2, pp. 997–1003, 2015.
[29] D. L. Buhr *et al.*, “Use of micro-emulsion technology for the directed evolution of antibodies,” *Methods*, vol. 58, no. 1, pp. 28–33, 2012.
[30] T. S. Kaminski, O. Scheler, and P. Garstecki, “Droplet microfluidics for microbiology: Techniques, applications and challenges,” *Lab Chip*, vol. 16, no. 12, pp. 2168–2187, 2016.
[31] H. Lee *et al.*, “A high-throughput optomechanical retrieval method for sequence-verified clonal DNA from the NGS platform,” *Nat. Commun.*, vol. 6, pp. 1–7, 2015.
[32] S. Kim *et al.*, “PHLI-seq: constructing and visualizing cancer genomic maps in 3D by phenotype-based high-throughput laser-aided isolation and sequencing,” *Genome Biol.*, vol. 19, no. 1, pp. 1–17, 2018.
[33] J. Noh *et al.*, “High-throughput retrieval of physical DNA for NGS-identifiable clones in phage display library,” *MAbs*, vol. 11, no. 3, pp. 532–545, 2019.
[34] J. Zhang *et al.*, “Sacrificial-layer free transfer of mammalian cells using near infrared femtosecond laser pulses,” *PLoS One*, vol. 13, no. 5, pp. 1–11, 2018.
[35] D. B. Weibel, W. R. Diluzio, and G. M. Whitesides, “Microfabrication meets microbiology.,” *Nat. Rev. Microbiol.*, vol. 5, no. 3, pp. 209–218, 2007.
[36] T. Ferreira and W. Rasband, “The ImageJ 1.44 User Guide,” *Manager*, pp. 1–199, 2011.
[37] Y. Wang *et al.*, “Micromolded arrays for separation of adherent cells.,” *Lab Chip*, vol. 10, no. 21, pp. 2917–2924, 2010.
[38] K. M. Choi and J. A. Rogers, “A photocurable poly(dimethylsiloxane) chemistry designed for soft lithographic molding and printing in the nanometer regime,” *J. Am. Chem. Soc.*, vol. 125, no. 14, pp. 4060–4061, 2003.
[39] M. D. Byoung Choul Kim, Christopher Moraes, Jiexi Huang, Toshiki Matsuoka and and S. T. Thouless, “Fracture-based Fabrication of Normally-closed, Adjustable and Fully Reversible Micro-scale Fluidic

Channels," *Small*, vol. 10, no. 19, pp. 4020–4029, 2014.
[40] P. Mathonet and C. G. Ullman, "The application of next generation sequencing to the understanding of antibody repertoires," *Front. Immunol.*, vol. 4, no. SEP, pp. 1–5, 2013.
[41] S. Kim *et al.*, "Efficient selection of antibodies reactive to homologous epitopes on human and mouse hepatocyte growth factors by next-generation sequencing-based analysis of the B cell repertoire," *Int. J. Mol. Sci.*, vol. 20, no. 2, 2019.
[42] R. S. Salvat *et al.*, "Computationally optimized deimmunization libraries yield highly mutated enzymes with low immunogenicity and enhanced activity," *Proc. Natl. Acad. Sci. U. S. A.*, vol. 114, no. 26, pp. 5085–5093, 2017.
[43] A. S. Dimitrov, *Therapeutic Antibodies Methods and Protocols*, vol. 53, no. 9. 2008.
[44] A. S. De Groot, M. Goldberg, L. Moise, and W. Martin, "Evolutionary deimmunization: An ancillary mechanism for self-tolerance?," *Cell. Immunol.*, vol. 244, no. 2, pp. 148–153, 2006.
[45] I. issues with therapeutic Proteins., "Immunogenicity issues with therapeutic proteins.," *Curr. Drug Discov. Technol.*, no. 12, pp. 20–24, 2004.

국문 초록

생명공학기술의 발전에 따라 바이오의약품의 성공률이 점차 증가하면서 제약회사들의 관심이 증가하고 있다. 특히 항체 의약품에 대한 관심이 증대되어 현재 제약시장을 선도하고 있으며, 향후 5~6년간 연성장률 12.8%를 보일 것으로 전망되고 있다. 따라서 항체 신약 개발의 중요도가 점차 올라가고 있다. 항체 신약 개발의 초기 장애물 중에 하나는 수백만 개의 후보군들 안에서 유의미한 몇 안되는 항체를 발굴하는 점이다.

Phage display 기술은 신약 개발 과정에서 항체 라이브러리 분석을 위해 가장 널리 쓰이는 방법이다. 다양한 항체 정보를 포함하는 phagemid 라이브러리를 phage의 표면에 발현하여, 유전형-표현형의 연결고리를 제공하여 항체의 선별과 분석을 용이하게 한다. Biopanning이라 불리는 과정을 통하여 특정한 항원과 높은 결합력을 갖는 항체를 강화하여 가장 높은 결합력을 가진 결합체를 여러 번의 biopanning을 거쳐 수많은 후보군들 속에서 선별하게 된다. 거대

라이브러리 분석이 가능한 높은 처리 용량과 손쉬운 분석 과정, 낮은 비용을 통한 뛰어난 분석 역량은 phage display가 항체 신약 발굴에서 가장 강력한 도구가 되게 했다.

이러한 장점들에도 불구하고, phage display는 소요 시간 및 비용, 강도 높은 노동, 제한된 분석 크기와 결합체의 손실과 같은 단점들이 있다. 첫 번째로, 노동력을 많이 필요로 하는 colony picking과 각각의 phage에 대한 기능 분석은 분석 가능한 라이브러리의 크기를 고작 수백개로 축소 시킨다(전체 라이브러리의 크기>10^9). 이러한 분석 가능한 라이브러리의 제한 때문에 특정 항원과 결합하는 클론들을 증폭시키기 위하여 biopanning 과정을 여러 번 반복하게 된다. 멀티채널 피펫 장비, 96웰 플레이트와 같은 자동화 장비를 통해 노동을 줄이려는 노력이 있었지만, 다수의 biopanning을 줄이기에 충분한 처리량을 제공하지 못했다.

또한 각각의 biopanning 과정에서 결합체의 손실이 발생하게 된다. 충분하지 않은 결합체의 용리로 인하여 높은 결합력을 가진 결합체는 손실되고, 증폭 과정에서의 편중으로 인하여 희귀 결합체 또한 손실된다. 자성입자의 이용을 통한 표면적의 증가로 인해 항체-항원 결합과정에서의 효율성을 증가 시킬 수 있었지만, 다른 과정에서는 별다른 효과가 없었다. 따라서 전 과정에서의 높은 처리량의 확보를

통하여 다수의 panning을 줄여, 소요 시간 및 비용, 결합체의 손실을 최소화 해야 한다.

생명과학 분야의 발전에 기여한 마이크로기술을 적용하기 위한 많은 노력이 있어왔다. 특히 phage display 적용을 위하여, 다양한 단일 세포 수준 분석법이 편향된 증폭을 최소화하고 처리량을 최대화 하여 다수의 panning을 감소시키는 방향으로 개발되었다. 높은 집약도로 이루어진 미세모세관 칩을 이용한 미세모세관 기술의 도입을 통해, 백만 개 이상의 항체들을 한번에 성공적으로 분석하였다. 또한 미세유체 기술을 도입하여 미세에멀젼을 통해 이론적으로 거의 무한에 가깝게 처리량을 증가하였다. 두 기술 모두 극도로 높은 처리량을 통해 다수의 panning을 줄이는 것에는 성공하였지만, 복잡한 샘플 회수 방법이 요구된다. 게다가 두 기술 모두 샘플 회수의 과정에서 교차 오염이 일어날 가능성이 높은 단점이 있다.

본 논문에서는 미세우물 어레이 칩과 자동화된 레이저 샘플 분리 장비를 이용하여 높은 처리량을 가진 phage display 기술을 개발하였다. 단일 세포 접근법과 정교한 샘플 분리 방법을 함께 적용하여 샘플의 교차 오염뿐만 아니라 증폭 과정에서의 편중을 최소화하고, 높은 처리량의 샘플 회수를 가능하게 하였다. 면역원성 제거를 목적으로 한 합성 항체 라이브러리를 기존의 biopanning 방식으로는 발굴할 수 없었던

새로운 항체 발굴을 위하여 개발된 phage display 기술로 분석하였다.

주요어 : 고속처리 phage display, 미세우물 어레이, 자동화 시스템, 항체 스크리닝
학번 : 2013-23138